

# Symmetry and Rigidity for Boosting Erbium-Based Molecular Light-Upconversion in Solution.

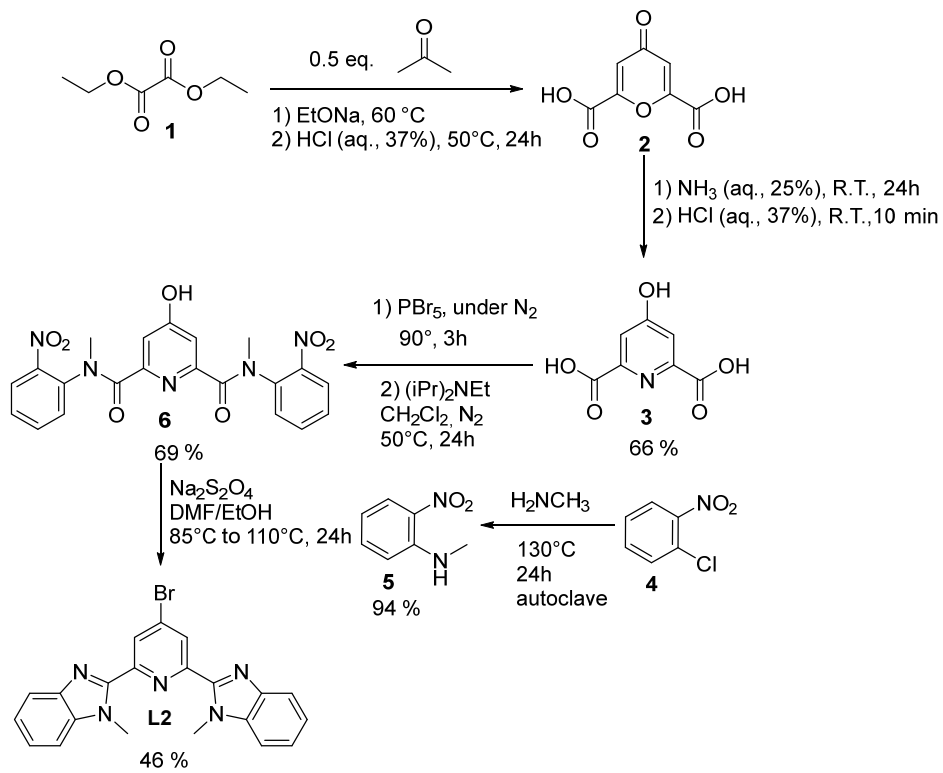
*Soroush Naseri,\* Inès Taarit,\* Hélène Bolvin, Jean-Claude Bünzli, Alexandre Fürstenberg, Laure Guénée, Giau Le-Hoang, Mohsen Mirzakhani, Homayoun Nozary, Arnulf Rosspeintner, Claude Piguet\**

## Supporting Information

(39 pages)

## Appendix 1. Experimental section

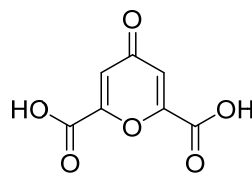
All commercial chemicals were purchased from Alfa Aesar, Aldrich, FluroChem, Acros, Fischer Chemicals AG and Sigma-Aldrich, and used without additional purification. Ligands **L1**, **L6-L8**<sup>[67]</sup> **L3-L5**,<sup>[66]</sup> and **L9**<sup>[68]</sup> were prepared according to literature. The hexafluoroacetylacetone salts [**digLn(hfa)<sub>3</sub>**] were synthesized from the corresponding oxide (Aldrich, 99.9%).<sup>[A1-1]</sup> Dichloromethane (DCM) and *N,N*-dimethylformamide were dried over calcium hydride. Silica gel plates Merck 60 F<sub>254</sub> were applied for thin layer chromatography, Silica gel glass plates Merck 60 F<sub>254</sub> were used for plate chromatography and Fluka silica gel 60 (0.04-0.063 mm) was used for preparative column chromatography.



**Scheme A1-1.** Synthetic pathway of **L2**.

### Preparation of chelidonic acid (**2**).

Dry ethanol (1 L) was prepared by adding CaH<sub>2</sub> (2 g) and refluxing overnight under an argon atmosphere. The solvent was then distilled under argon. In a similar way, acetone (50 g, 63.8 mL, 0.86 mol, 1 equiv.) was dried by adding K<sub>2</sub>CO<sub>3</sub> (20 g) and refluxed overnight under an argon atmosphere. The solvent was then distilled under argon. Sodium (62 g, 2.7 mol, 3.14 equiv.) was slowly dissolved in the distilled dry ethanol. Diethyl oxalate (267.1 g, 246 mL, 1.83 mol, 2.13 equiv.) was added to the distilled acetone, and this mixture was added dropwise to the sodium ethanolate solution. A yellow-

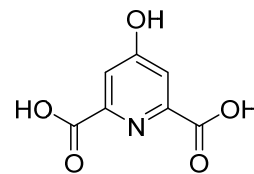


orange precipitate was formed. The mixture was stirred at 60°C for 1 hour. Then, HCl (aq. 37%, 530 mL) and water (250 mL) were added, and the solution stirred at 50°C for 1 day. Around 1 L of ethanol-water mixture was removed by evaporation under reduced pressure and then a mixture of water (600 mL) and HCl (aq. 37%, 140 mL) was added while stirred and heated at 50°C until a silica gel TLC (eluent: 3/7 (v/v) 10% NaCl/ethanol) showed only one spot for the desired product. After 3 days of reaction, the mixture was cooled to room temperature, the solid was filtered off, washed a first time with water (100 mL) and then with cold acetone (100 mL). The crude wet product (296.87 g) was used directly for the next step without any further purification. A small amount of the crude product (291 mg) was dissolved in boiling water (7 mL) and charcoal was added. The mixture was refluxed for 15 minutes and then filtered over celite (diatomaceous earth) and gave 56.4 mg of **2** as a pure beige powder.

<sup>1</sup>H NMR (400 MHz, DMSO-d<sub>6</sub>): δ 6.88 (s, 2H). ESI-MS (CHCl<sub>3</sub>) *m/z*: 185.0 ([M+H]<sup>+</sup>).

#### Preparation of chelidamic acid (**3**).

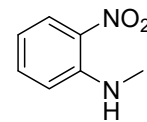
The crude wet chelidonic acid (**2**, 296.52 g) was put in a 2 L flask and hydroxide ammonium (NH<sub>3</sub> 25%, 1.5 L) was added dropwise while keeping it stirred at 0°C. It was then stirred for 48 hours at room temperature. The mixture went from orange to beige after about 1 hour and finally turned to dark orange over the first night. The excess of ammonia was removed completely by boiling the mixture and the released gas was quenched over a water trap. Charcoal (30 g) was added to the mixture and boiled for 1 hour. The mixture was then filtered and cooled to about 5°C. The solution was then acidified to pH = 1 with an HCl solution (37%). The pale brown crystals (expected white) were filtered off and washed several times with ice-cold water and dried overnight under vacuum at 50°C to give chelidamic acid (**3**, 103.63 g, 0.57 mol, yield over 2 steps = 65.7%). A part of the crude product (25.60 g) was purified by dissolving it in 200 mL of NH<sub>4</sub>OH (25%) and the mixture was kept at pH = 9-10. The solution was washed with CH<sub>2</sub>Cl<sub>2</sub> (3x150 mL), the aqueous phase was isolated, and the final product was precipitated by adding a HCl solution (37%) until pH = 1 and stirred for 10 minutes. The crystals were filtered, washed with ice-cold water, and then dried overnight under vacuum at 65°C to give 21.83 g of chelidamic acid (**3**).



<sup>1</sup>H NMR (400 MHz, DMSO-d<sub>6</sub>): δ 7.56 (s, 2H). ESI-MS (CHCl<sub>3</sub>) *m/z*: 184.0 ([M+H]<sup>+</sup>).

#### Preparation of *N*-methyl-2-nitroaniline (**5**).

1-Chloro-2-nitrobenzene (**4**, 10.3199 g, 65.5 mmol, 1 equiv.) and methylamine (65.3 mL, 40% in water, 1.9 equiv.) were heated in an autoclave at 130°C for 24 h. The dark mixture (2 phases: red on top and black on bottom) was evaporated to dryness and partitioned between dichloromethane (50 mL) and aqueous NH<sub>4</sub>Cl solution (50 mL, half-saturated).

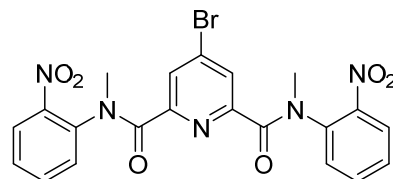


The organic layer was separated, and the aqueous phase further extracted with CH<sub>2</sub>Cl<sub>2</sub> (2x50 mL). The combined organic phases were dried over Na<sub>2</sub>SO<sub>4</sub>, evaporated to dryness and the crude product purified by column chromatography (Silicagel, CH<sub>2</sub>Cl<sub>2</sub> 100%) to give **5** (9.3688 g, yield: 94%).

<sup>1</sup>H NMR (400 MHz, Methylene Chloride-d<sub>2</sub>): δ 8.18 (dd, J = 8.7, 1.6 Hz, 1H), 8.04 (s, 1H), 7.52 (dddd, J = 8.6, 6.9, 1.6, 0.7 Hz, 1H), 6.92 (dd, J = 8.7, 1.3 Hz, 1H), 6.70 (ddd, J = 8.4, 6.9, 1.3 Hz, 1H), 3.06 (d, J = 5.1 Hz, 3H).

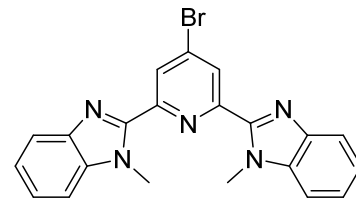
#### Preparation (one-pot) of 4-bromo-N<sup>2</sup>,N<sup>6</sup>-dimethyl-N<sup>2</sup>,N<sup>6</sup>-bis(2-nitrophenyl) pyridine-2,6-dicarboxamide (**6**).

Chelidamic acid (**3**, 3.016 g, 16.47 mmol, 1 equiv.) was added to a 50 mL flask containing PBr<sub>5</sub> (11.42 g, 26.53 mmol, 1.62 equiv.). The temperature was raised to 90°C for 3h under nitrogen. The mixture was cooled to room temperature and dissolved with dry CH<sub>2</sub>Cl<sub>2</sub> (75 mL) and filtered (under N<sub>2</sub>) and directly added to a solution of *N*-methyl-2-nitroaniline (5.2 g, 34.18 mmol, 2.09 equiv.) and (i-Pr)<sub>2</sub>NEt (15 mL) in dry CH<sub>2</sub>Cl<sub>2</sub> (30 mL). The mixture was stirred at reflux for 24 h. The pH was adjusted to 7 by addition of (i-Pr)<sub>2</sub>NEt, and the reaction mixture was evaporated to dryness. The crude product was purified by column chromatography (SiO<sub>2</sub>, CH<sub>2</sub>Cl<sub>2</sub>/MeOH 100: 0 → 99.5: 0.5) to give **6** (2.6776 g, 48%) as a yellowish microcrystalline powder and unreacted *N*-methyl-2-nitroaniline was also recovered.



#### Preparation of 2,6-bis(1'-methyl-benzimidazol-2'-yl)-4-bromopyridine (**L2**).

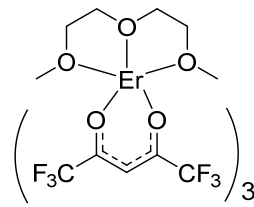
A solution of 4-bromo-N<sup>2</sup>,N<sup>6</sup>-dimethyl-N<sup>2</sup>,N<sup>6</sup>-bis(2-nitrophenyl) pyridine-2,6-dicarboxamide (**6**, 2.78 g, 5.41 mmol, 1 equiv.) and Na<sub>2</sub>S<sub>2</sub>O<sub>4</sub> (9.98 g, 57.32 mmol, 11 equiv.) in DMF (75 mL) and EtOH (50 mL) was stirred and warm up to 85°C. Then, H<sub>2</sub>O (50 mL) was added, and the reaction mixture was stirred at reflux (110°C) for 24 h. The mixture was evaporated to dryness, suspended in CH<sub>2</sub>Cl<sub>2</sub> (100 mL) in a separating funnel and an aqueous NaHCO<sub>3</sub> solution (100 mL, half-saturated, pH = 8-9) was added. A saturated aqueous NaCl solution was then added to help the formation of two phases in the separatory funnel and the organic phase was extracted (4x100mL) with CH<sub>2</sub>Cl<sub>2</sub>. The combined organic phases were washed with an aqueous NaHCO<sub>3</sub> solution (50 mL, half-saturated, pH = 8-9), dried over Na<sub>2</sub>SO<sub>4</sub>, filtered, and evaporated to dryness. The crude product was purified by column chromatography (Silicagel, CH<sub>2</sub>Cl<sub>2</sub> 100%→CH<sub>2</sub>Cl<sub>2</sub>/Methanol 99:1) to give (**L2**, 1.04 g, yield: 46%).



<sup>1</sup>H NMR (400 MHz, Chloroform-d): δ 8.65 (s, 2H), 7.93 – 7.85 (m, 2H), 7.53 – 7.47 (m, 2H), 7.46 – 7.36 (m, 4H), 4.27 (s, 6H). ESI-MS (CHCl<sub>3</sub>) *m/z*: 417.7 ([M+H]<sup>+</sup>).

### Preparation of [digEr(hfa)<sub>3</sub>].

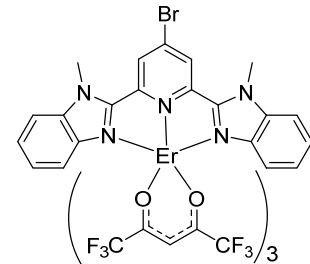
Erbium oxide (2.0 g, 5.25 mmol, 1 equiv.) was suspended in water (5 mL) and nitric acid (3 mL, 65%) was added. The mixture was stirred at reflux until a clear solution was obtained and then cooled down. A solution of NaOH (4 M) was added until complete neutralization and a pinkish precipitate appears. The precipitate was filtered and dried under vacuum to yield 2.05 g of Er(OH)<sub>3</sub>·xH<sub>2</sub>O. Diglyme (1.39 mL, 9.39 mmol, 1 equiv.) was added to a suspension of the erbium hydroxide (1 equiv.) in toluene (200 mL). Hexafluoroacetylacetone (Hhfa) (3.99 mL, 28.9 mmol, 3 equiv.) was added after 10 minutes under vigorous stirring and the mixture was refluxed for 3 h. Once the erbium hydroxide was completely reacted and the solution was clear, the solvent was removed under vacuum. The resulting pink waxy oil was sublimed (10<sup>-5</sup> mbar / 55°C) to yield a pink crystalline powder, which was then recrystallized in hexane (300 mL) affording pink X-ray quality crystals of [digEr(hfa)<sub>3</sub>]·0.2H<sub>2</sub>O (3.65 g, 3.96 mmol, yield: 38%).



<sup>1</sup>H NMR (400 MHz, Chloroform-d): δ 141.45 (s, 0H), 73.02 (s, 2H), 23.25 (s, 2H), -48.51 (s, 1H). <sup>19</sup>F NMR (376 MHz, Chloroform-d): δ -99.14. Elemental analysis for [digEr(hfa)<sub>3</sub>]·0.2H<sub>2</sub>O (calc. C 27.23, H 1.89, N 0.0; found C 27.28, H 1.95, N 0.02).

### Preparation of [L2Er(hfa)<sub>3</sub>].

Stoichiometric amounts of **L2** (0.036 mmol, 1.0 equiv.) and Er(hfa)<sub>3</sub>·dig·1.35 H<sub>2</sub>O (0.036 mmol, 1.0 equiv.) were dissolved and stirred in dichloromethane/acetonitrile (1:1, 3 mL). Slow diffusion of diethyl ether into a concentrated solution/slow evaporation of dichloromethane provided pink X-ray quality crystals of [L2Er(hfa)<sub>3</sub>] (30 mg, 0.025 mmol, yield: 69%).



Elemental analysis for [L2Er(hfa)<sub>3</sub>] calc. C 35.83, H 1.59, N 5.80; found C 35.81, H 1.61, N 5.75.

### Spectroscopic and analytical measurements

<sup>1</sup>H NMR spectra were recorded at 293 K on a Bruker Avance 400 MHz spectrometer. Chemical shifts are given in ppm with respect to tetramethylsilane Si(CH<sub>3</sub>)<sub>4</sub>(TMS). Spectral assignment was assisted by 2D COSY NMR experiment where appropriate. Pneumatically-assisted electrospray (ESI) mass spectra were recorded from 10<sup>-4</sup> M solutions on an API 150EX (AB/MDS Sciex) equipped with a Turbo Ionspray source<sup>®</sup>. Elemental analyses were performed by K. L. Paglia from the Microchemical Laboratory of the University of Geneva.

Emission spectra were measured on a Horiba Scientific Fluorolog 3 spectrofluorometer equipped with a visible photomultiplier tube (PMT) (220-850 nm, R928P, Hamamatsu). The infrared luminescence spectra were recorded using a NIR-PMT cooled to -80 °C (300-1700 nm, R5509-73,

Hamamatsu) and an 850 nm longpass filter (Thorlabs) upon 801 nm laser excitation. The fluorescence intensities were corrected when transposed to the wavenumber scale according to  $F(\tilde{\nu}) \propto \lambda^2 F(\lambda)$ .<sup>[A1-2]</sup> The standard xenon lamp of the Horiba Scientific Fluorolog 3 spectrofluorometer was used for UV excitation of the samples to record the pertinent emission spectra, where the appropriate longpass filters (Thorlabs) were placed after the sample to remove the second-order Rayleigh scattering of the xenon lamp. The emission spectra were corrected for the instrumental response function. Continuous NIR laser excitation was achieved with a diode laser MLL-H-800-2.5W (801 nm) from Changchun New Industries Optoelectronics Technology Co., Ltd (CNI). A 550/88 nm bandpass filter (Semrock) was placed directly after the sample for visible emission measurements to remove the first and second-order Rayleigh scattering and potentially reduce straylight in the monochromator from the massive scattering. Excitation into the ligand-centered  $\pi_1^* \leftarrow \pi$  transition was performed with a diode laser at  $\lambda_{\text{exc}} = 401$  nm (BrixX® 405-1200 HP) manufactured by Omicron-Laserage. The excitation beam was loosely focused onto the sample with a 30 cm lens to reach an excitation spot size of  $\approx 1.5$  mm in diameter (Surface  $\approx 0.07$  cm<sup>2</sup>). The mathematical analyses were performed by using Igor Pro® (WaveMetrics Inc.), Origin 2017 (OriginLab Corporation) and Excel® (Microsoft) software. The upconversion quantum yields were determined through the relative method using indocyanine green as the reference (ICG,  $\lambda_{\text{exc}} = 801$  nm,  $\Phi^{\text{ref}} = 0.132$  in ethanol at 293 K,  $n_{\text{acetonitrile}} = 1.344$ ).<sup>[A1-3]</sup> Quantitative data for the upconversion process were obtained by using indocyanine green and eqn. (2), where  $\Phi$  is the quantum yield,  $E$  is the integrated emission spectrum,  $A$  is the absorbance at the excitation wavelength  $\lambda$ ,  $n$  is the refractive index ( $n_{\text{DCM}} = 1.424$ ,  $n_{\text{acetonitrile}} = 1.344$ , and  $n_{\text{ethanol}} = 1.361$ ),  $P_{\text{exc}}$  is the power intensity of the excitation source at the excitation wavelength and  $h\nu_{\text{exc}}$  is the energy of the incident photon at frequency  $\nu_{\text{exc}} = (c/\lambda_{\text{exc}})$  so that  $I_{\text{exc}} = P_{\text{exc}}/h\nu_{\text{exc}}$  is the spectral radiant power measuring the incident excitation intensity.<sup>[A1-4]</sup>

$$\frac{\Phi^{\text{up}}}{\Phi^{\text{ref}}} = \frac{E_{\text{up}}}{E_{\text{ref}}} \cdot \frac{A_{\text{ref}}}{A_{\text{up}}} \cdot \frac{n_{\text{ref}}^2}{n_{\text{up}}^2} \cdot \frac{P_{\text{exc,ref}}}{P_{\text{exc,up}}} \cdot \frac{h\nu_{\text{exc,up}}}{h\nu_{\text{exc,ref}}} \quad (\text{A1-1})$$

The geometry of the measuring cell was fixed (position and rotation) for recording the upconversion emission spectra. The indocyanine green reference was then measured in the same conditions and extreme care were taken for having identical location of the incident beam and detector. The concentration of the reference was adapted so that its emission intensity was comparable with that of the sample using the same excitation power. During the experiments for the sake of precision of the measurement (particularly for recording the green upconverted signal), the whole room was in total darkness. Electronic absorption spectra in the Visible and NIR regions were recorded at 293 K from dichloromethane (acetonitrile for  $[\text{L2Er(hfa)}_3]$  and  $[\text{Er(Et-bzimpy)}_3]^{3+}$ , and ethanol for ICG) solutions with a Perkin-Elmer Lambda 1050 absorption spectrometer using quartz cell of 0.1, 1- and 10-mm

path length. Solution emission spectra were recorded in non-deuterated dichloromethane (non-deuterated acetonitrile for  $[\text{L2Er(hfa)}_3]$  and  $[\text{Er(Et-bzimpy)}_3]^{3+}$ , and non-deuterated ethanol for ICG) using quartz cells of 5 mm path length. The emission spectrum of ICG was recorded upon excitation at  $\lambda_{\text{exc}} = 705$  nm using the standard xenon lamp of the Horiba Scientific Fluorolog 3 spectrofluorimeter. The emission spectra were corrected for the instrumental response function.

The ultrafast time-gated experiments used a pulsed laser as excitation light source (355 nm, CNI Laser MPL-F-355). A 390 nm shortpass filter was used in order to spectrally clean the light source. The polarization of the excitation was controlled using a Glan-Taylor polarizer and set to s-polarization. Fluorescence of the samples was collected using a Cassegrain type collection optic (Anagrain; Anaspec Research Laboratories Ltd., Berkshire, UK) in 180-back-scattering geometry, passed through a wire-grid polarizer (Thorlabs, WP25M\_UB) at magic angle with respect to the excitation, and focused onto a fiber using an off-axis parabolic mirror (Thorlabs, MPD149-P01). A Triax-190 (Horiba) imaging spectrograph with a 150 lines/mm grating ( $\lambda_{\text{blaze}} = 500$  nm) was used to disperse the fluorescence coming from the multimode fiber (200  $\mu\text{m}$ , NA 0.12, CeramOptec). For all samples a detection wavelength of 542 nm and a bandpass of approx. 2 nm was used. The spectrally dispersed light exiting the spectrograph was focused on a cooled photomultiplier (Picoquant, PMA-192-C). The time-correlated single photon counting was performed with a quTAG MC (quTools).

### X-ray crystallography

Summary of crystal data, intensity measurements and structure refinements for the complexes  $[\text{digEr(hfa)}_3]$  and  $[\text{L2Er(hfa)}_3]$  were collected in Tables S2 and S4 in the SI. Pertinent bond lengths, bond angles and interplanar angles were collected (Tables S3, S5) together with ORTEP views (Figures S2-S3). Crystals were mounted on Hampton cryoloops with protection oil. X-ray data collections were performed with a XtaLAB Synergy-S diffractometer equipped with a hybrid pixel array “hypix arc 150” detector. The structures were solved with ShelXT<sup>[A1-5]</sup> and all other calculations were performed with SHELLXL,<sup>[A1-6]</sup> OLEX2<sup>[A1-7]</sup> and ORTEP<sup>[A1-8]</sup> programs. CCDC 2292314-2292315 contain the supplementary crystallographic data for this paper. These data can be obtained free of charge from The Cambridge Crystallographic Data Centre via [www.ccdc.cam.ac.uk/data\\_request/cif](http://www.ccdc.cam.ac.uk/data_request/cif).

### Bond valence calculations.

One can delve into the structural analysis while using bond valence calculations (eq A1-2) for evaluating metal-ligand affinities and ligand distortions in the solid state, where  $v_{ij}$  is the bond valence measuring the affinity is assigned to each interaction pair formed by a donor  $j$  and a central atom  $i$ .<sup>[A1-9],[A1-10]</sup> According to eq (A1-2),  $v_{ij}$  is related to the bond length of the interaction pair ( $d_{ij}$ ) whereby

$R_{ij}$  is known as the bond valence parameter, which only depends on a pair of interacting atoms, and  $b = 0.37$  is a universal scaling constant.<sup>[A1-11],[A1-12]</sup>

$$\nu_{ij} = e^{[(R_{ij} - d_{ij})/b]} \quad (\text{A1-2})$$

Having accurate values for  $R_{\text{Ln-O}}$ <sup>[A1-12],[A1-14]</sup> and  $R_{\text{Ln-N}}$ <sup>[A1-15]</sup> for nine-coordinate complexes along the lanthanide series, eq (A1-2) provides  $\nu_{\text{Ln-O}}$  and  $\nu_{\text{Ln-N}}$  bond valences associated with each  $[\text{LkLn(hfa)}_3]$  complex (Tables S7-S9, Figure S5).

## References

- [A1-1] a) W. J. Evans, D. G. Giarikos, M. A. Johnston, M. A. Grecian, J. W. Ziller, *J. Chem. Soc., Dalton Trans.* **2002**, 520-526; b) G. Malandrino, R. Lo Nigro, I. L. Fragalà, C. Benelli, *Eur. J. Inorg. Chem.* **2004**, 500-509; c) G. Malandrino, I. L. Fragalà, *Coord. Chem. Rev.* **2006**, 250, 1605-1620; d) A. Valore, E. Cariati, S. Righetto, D. Roberto, F. Tessore, R. Ugo, I. L. Fragalà, M. E. Fragalà, G. Malandrino, F. De Angelis, L. Belpassi, I. Ledoux-Rak, K.-H. Thi, J. Zyss, *J. Am. Chem. Soc.* **2010**, 132, 4966-4970.
- [A1-2] G. Angulo, G. Grampp, A. Rosspeintner, *Spectrochimica Acta Part A* **2006**, 65, 727-731
- [A1-3] K. Rurack, M. Spieles, *Anal. Chem.* **2011**, 83, 1232-1242.
- [A1-4] a) J. W. Verhoeven, *Pure and Appl. Chem.* **1996**, 68, 2223-2286; b) C. Wurth, M. Grabolle, J. Pauli, M. Spieles and U. Resch-Genger, *Nature Protocols* **2013**, 8, 1535-1550.
- [A1-5] G. M. Sheldrick, *Acta Crystallogr. C: Structural Chemistry* **2015**, 71, 3-8.
- [A1-6] G. M. Sheldrick, *Acta Crystallogr. A* **2008**, 64, 112-122.
- [A1-7] O. V. Dolomanov, L. J. Bourhis, R. J. Gildea, J. A. K. Howard, H. Puschmann, *J. Appl. Crystallogr.* **2009**, 42, 339-341.
- [A1-8] L. Farrugia, *J. Appl. Crystallogr.* **1997**, 30, 565.
- [A1-9] A. Zaïm, H. Nozary, L. Guénée, C. Besnard, J.-F. Lemonnier, S. Petoud, C. Piguet, *Chem. Eur. J.* **2012**, 18, 7155-7168.
- [A1-10] A. Escande, L. Guénée, K.-L. Buchwalder, C. Piguet, *Inorg. Chem.* **2009**, 48, 1132-1147.
- [A1-11] I. D. Brown, D. Altermatt, *Acta Cryst. B*, **1985**, 41, 244-247.
- [A1-12] I. D. Brown, *Chem. Rev.* **2009**, 109, 6858-6919.
- [A1-13] A. Trzesowska, R. Kruszynski, T. J. Bartczak, *Acta Cryst B Structural Science* **2004**, B60, 174-178.
- [A1-14] F. Zocchi, *J. Mol. Struct. Theochem.* **2007**, 805, 73-78.
- [A1-15] A. Trzesowska, R. Kruszynski, T. J. Bartczak, *Acta Cryst B Structural Science* **2005**, B61, 429-434.

$$\begin{pmatrix} -k_A^{\text{exc}(0 \rightarrow 1)} & k_A^{1 \rightarrow 0} & k_A^{2 \rightarrow 0} \\ k_A^{\text{exc}(0 \rightarrow 1)} & -(k_A^{\text{exc}(1 \rightarrow 2)} + k_A^{1 \rightarrow 0}) & k_A^{2 \rightarrow 1} \\ 0 & k_A^{\text{exc}(1 \rightarrow 2)} & -(k_A^{2 \rightarrow 1} + k_A^{2 \rightarrow 0}) \end{pmatrix} \times \begin{pmatrix} N_{\text{A,S-S}}^{|0\rangle} \\ N_{\text{A,S-S}}^{|1\rangle} \\ N_{\text{A,S-S}}^{|2\rangle} \end{pmatrix} = \begin{pmatrix} 0 \\ 0 \\ 0 \end{pmatrix} \quad (\text{S1})$$

$$N^{\text{tot}} = N_{\text{A,S-S}}^{|0\rangle} + N_{\text{A,S-S}}^{|1\rangle} + N_{\text{A,S-S}}^{|2\rangle} = 1 \quad (\text{S2})$$

$$N_{\text{A,S-S}}^{|0\rangle} = \frac{k_A^{1 \rightarrow 0} (k_A^{2 \rightarrow 1} + k_A^{2 \rightarrow 0}) + k_A^{\text{exc}(1 \rightarrow 2)} k_A^{2 \rightarrow 0}}{(k_A^{\text{exc}(0 \rightarrow 1)} + k_A^{1 \rightarrow 0})(k_A^{2 \rightarrow 1} + k_A^{2 \rightarrow 0}) + k_A^{\text{exc}(1 \rightarrow 2)} (k_A^{\text{exc}(0 \rightarrow 1)} + k_A^{2 \rightarrow 0})} \approx 1 \quad (\text{S3})$$

$$N_{\text{A,S-S}}^{|1\rangle} = \frac{k_A^{\text{exc}(0 \rightarrow 1)} (k_A^{2 \rightarrow 1} + k_A^{2 \rightarrow 0})}{(k_A^{\text{exc}(0 \rightarrow 1)} + k_A^{1 \rightarrow 0})(k_A^{2 \rightarrow 1} + k_A^{2 \rightarrow 0}) + k_A^{\text{exc}(1 \rightarrow 2)} (k_A^{\text{exc}(0 \rightarrow 1)} + k_A^{2 \rightarrow 0})} \approx \frac{k_A^{\text{exc}(0 \rightarrow 1)}}{(k_A^{1 \rightarrow 0})} \quad (\text{S4})$$

$$N_{\text{A,S-S}}^{|2\rangle} = \frac{k_A^{\text{exc}(0 \rightarrow 1)} k_A^{\text{exc}(1 \rightarrow 2)}}{(k_A^{\text{exc}(0 \rightarrow 1)} + k_A^{1 \rightarrow 0})(k_A^{2 \rightarrow 1} + k_A^{2 \rightarrow 0}) + k_A^{\text{exc}(1 \rightarrow 2)} (k_A^{\text{exc}(0 \rightarrow 1)} + k_A^{2 \rightarrow 0})} \approx \frac{k_A^{\text{exc}(0 \rightarrow 1)} k_A^{\text{exc}(1 \rightarrow 2)}}{(k_A^{1 \rightarrow 0})(k_A^{2 \rightarrow 1} + k_A^{2 \rightarrow 0})} \quad (\text{S5})$$

**Scheme S1** Steady-state population density in the  $|i\rangle$  level  $N_{\text{A,S-S}}^{|i\rangle}$  (eqs S3-S5) obtained by solving the differential matrix equation pertinent to the single-center ESA mechanism for the  $[dN_{\text{S-S,A}}^{|i\rangle}/dt] = 0$  (eq S1) under continuous excitation pumping and with the explicit help of the mass balance (eq S2). Under weak incident excitation power used for inducing linear upconversion in molecular complexes ( $P = 0.1\text{-}40 \text{ W}\cdot\text{cm}^{-2}$ ),  $k_A^{\text{exc}(i \rightarrow j)}$  ( $\approx 1 \text{ s}^{-1}$ )  $\ll k_A^{j \rightarrow i}$  ( $\approx 10^5 \text{ s}^{-1}$ ) and a negligible number of molecules exist in the excited levels so that  $N_{\text{A,S-S}}^{|0\rangle} \approx N^{\text{tot}} = 1$  (eq S3). The associated approximations for  $N_{\text{A,S-S}}^{|1\rangle}$  and  $N_{\text{A,S-S}}^{|2\rangle}$  are shown at the end of eq (S4) and (S5), respectively.

**Table S1.** Thermodynamic stability constants  $\beta_{l,l}^{Lk,Ln}$  and ligand speciation for  $|Lk|_{tot}/|Eu(hfa)_3|_{tot} = 1.0$  determined from the titrations of  $Lk$  with  $[digLn(hfa)_3]$  in  $CD_2Cl_2$  at 293 K.<sup>[a]</sup>

Adduct	$\beta_{l,l,exch}^{Lk,Eu}$	% $[LkEu(hfa)_3]$	$\beta_{l,l,exch}^{Lk,Y}$	% $[LkY(hfa)_3]$	Reference
$[L1Ln(hfa)_3]$	374(36)	95	281(60)	94	[67]
$[L3Ln(hfa)_3]$	593(58)	96	—	—	[66]
$[L4Ln(hfa)_3]$	383(24)	95	—	—	[66]
$[L5Ln(hfa)_3]$	180(5)	93	—	—	[66]
$[L6Ln(hfa)_3]$	624(256)	96	509(210)	96	[67]
$[L7Ln(hfa)_3]$	$2.8(1.4)\cdot 10^3$	98	$1.5(6)\cdot 10^3$	97	[67]
$[L9Ln(hfa)_3]$	$2.2(8)\cdot 10^3$	98	$1.5(8)\cdot 10^3$	97	[68]



**Table S2.** Crystal data and structure refinement for the complex [digEr(hfa)<sub>3</sub>].

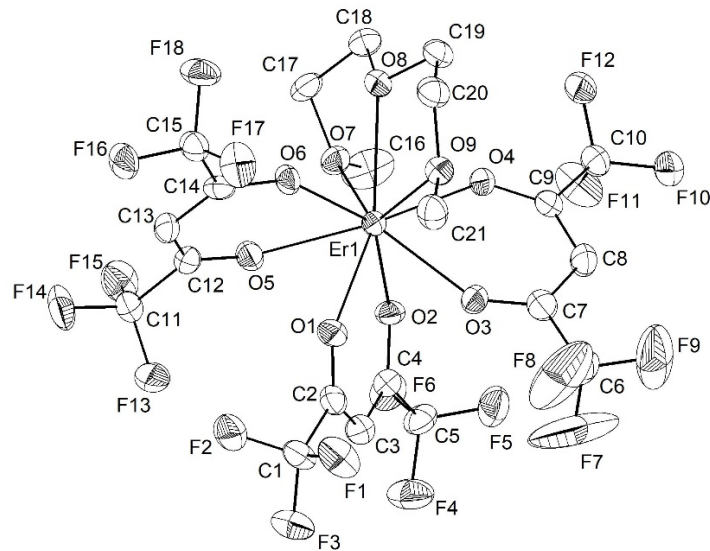
Compound	[digEr(hfa) <sub>3</sub> ]
Empirical formula	C <sub>21</sub> H <sub>17</sub> ErF <sub>18</sub> O <sub>9</sub>
Formula weight	922.60
Temperature	100.00(10) K
Wavelength	1.54184 Å
Crystal system	Monoclinic
Space Group	<i>P</i> 2 <sub>1</sub>
Unit cell dimensions	<i>a</i> = 9.27679(7) Å <i>b</i> = 18.60642(12) Å <i>c</i> = 9.43780(8) Å α = 90° β = 112.2019(9)° γ = 90°
Volume	1508.26(2) Å <sup>3</sup>
Z	2
Density (calculated)	2.032 Mg/m <sup>3</sup>
Absorption coefficient	6.670 mm <sup>-1</sup>
<i>F</i> (000)	890
Crystal size	0.18 x 0.17 x 0.12 mm <sup>3</sup>
Theta range for data collection	4.753 to 75.006°.
Index ranges	-7<= <i>h</i> <= 11, -22 <= <i>k</i> <= 22, -11 <= <i>l</i> <= 11
Reflections collected	22764
Independent reflections	6012 [ <i>R</i> (int) = 0.0370]
Completeness to theta = 67.684°	100.0 %
Absorption correction	Analytical
Max. and min. transmission	0.593 and 0.409
Refinement method	Full-matrix least-squares on F <sup>2</sup>
Data / restraints / parameters	6012 / 1 / 445
Goodness-of-fit on F <sup>2</sup>	1.029
Final <i>R</i> indices [ <i>I</i> >2sigma( <i>I</i> )]	<i>R</i> 1 = 0.0331, w <i>R</i> 2 = 0.0882
<i>R</i> indices (all data)	<i>R</i> 1 = 0.0333, w <i>R</i> 2 = 0.0884
Absolute structure parameter	0.354(12)
Largest diff. peak and hole	0.902 and -1.146 e.Å <sup>-3</sup>

**Table S3.** Selected bond distances ( $\text{\AA}$ ) and bond angles ( $^\circ$ ) for the complex  $[\text{digEr(hfa)}_3]$ .

Bond Distances / $\text{\AA}$					
Atom	Atom	Length/ $\text{\AA}$	Atom	Atom	Length/ $\text{\AA}$
Er(1)	O(1)	2.342(4)	Er(1)	O(6)	2.331(4)
Er(1)	O(2)	2.284(4)	Er(1)	O(7)	2.467(4)
Er(1)	O(3)	2.368(4)	Er(1)	O(8)	2.498(5)
Er(1)	O(4)	2.331(4)	Er(1)	O(9)	2.482(4)
Er(1)	O(5)	2.401(4)			

Bond Angles ( $^\circ$ )							
Atom	Atom	Atom	Angle / $^\circ$	Atom	Atom	Atom	Angle / $^\circ$
O(1)	Er(1)	O(3)	67.86(16)	O(4)	Er(1)	O(3)	72.27(15)
O(1)	Er(1)	O(5)	68.59(16)	O(4)	Er(1)	O(5)	134.87(15)
O(1)	Er(1)	O(7)	131.89(16)	O(4)	Er(1)	O(6)	138.75(15)
O(1)	Er(1)	O(8)	146.05(15)	O(4)	Er(1)	O(7)	72.39(15)
O(1)	Er(1)	O(9)	96.36(15)	O(4)	Er(1)	O(8)	71.04(15)
O(2)	Er(1)	O(1)	76.59(15)	O(4)	Er(1)	O(9)	81.85(15)
O(2)	Er(1)	O(3)	73.54(16)	O(5)	Er(1)	O(7)	66.49(15)
O(2)	Er(1)	O(4)	78.00(15)	O(5)	Er(1)	O(8)	106.33(15)
O(2)	Er(1)	O(5)	74.86(15)	O(5)	Er(1)	O(9)	139.71(14)
O(2)	Er(1)	O(6)	142.18(15)	O(6)	Er(1)	O(1)	76.74(16)
O(2)	Er(1)	O(7)	75.99(15)	O(6)	Er(1)	O(3)	119.25(16)
O(2)	Er(1)	O(8)	136.09(15)	O(6)	Er(1)	O(5)	70.68(15)
O(2)	Er(1)	O(9)	139.94(15)	O(6)	Er(1)	O(7)	103.36(15)
O(3)	Er(1)	O(5)	130.65(16)	O(6)	Er(1)	O(8)	70.22(15)
O(3)	Er(1)	O(7)	137.09(15)	O(6)	Er(1)	O(9)	69.50(14)
O(3)	Er(1)	O(8)	122.74(15)	O(7)	Er(1)	O(8)	65.53(15)
O(3)	Er(1)	O(9)	67.44(15)	O(7)	Er(1)	O(9)	129.40(14)
O(4)	Er(1)	O(1)	137.26(15)	O(9)	Er(1)	O(8)	65.14(14)



**Figure S1.** Ortep view of  $[\text{digEr}(\text{hfa})_3]$  (thermal ellipsoids are drawn at 50% probability level) with numbering scheme. Hydrogen atoms are omitted for clarity reason.

**Table S4.** Crystal data and structure refinement for the complex [L2Er(hfa)<sub>3</sub>].

Compound	[L2Er(hfa) <sub>3</sub> ]
Empirical formula	C <sub>40</sub> H <sub>25</sub> BrErF <sub>18</sub> N <sub>7</sub> O <sub>6</sub>
Chemical formula moiety	C <sub>36</sub> H <sub>19</sub> BrErF <sub>18</sub> N <sub>5</sub> O <sub>6</sub> , 2(C <sub>2</sub> H <sub>3</sub> N)
Formula weight	1288.84
Temperature	120.0(2) K
Wavelength	1.54184 Å
Crystal system	Orthorhombic
Space group	<i>F d d 2</i>
	<i>a</i> = 53.1339(3) Å
	<i>b</i> = 30.69026(15) Å
	<i>c</i> = 11.69971(6) Å
Unit cell dimensions	$\alpha$ = 90°
	$\beta$ = 90°
	$\gamma$ = 90°
Volume	19078.62(17) Å <sup>3</sup>
Z	16
Density (calculated)	1.795 Mg/m <sup>3</sup>
Absorption coefficient	5.377 mm <sup>-1</sup>
<i>F</i> (000)	10032
Crystal size	0.26 x 0.21 x 0.09 mm <sup>3</sup>
Theta range for data collection	3.326 to 74.727°
Index ranges	-66<=h<=65, -31<=k<=38, -14<=l<=14
Reflections collected	77382
Independent reflections	9526 [ <i>R</i> (int) = 0.0232]
Completeness to theta = 39.997°	100 %
Absorption correction	Analytical
Max. and min. transmission	0.674 and 0.431
Refinement method	Full-matrix least-squares on <i>F</i> <sup>2</sup>
Data / restraints / parameters	9526 / 1 / 691
Goodness-of-fit on <i>F</i> <sup>2</sup>	1.024
Final <i>R</i> indices [ <i>I</i> >2sigma( <i>I</i> )]	<i>R</i> <sub>1</sub> = 0.0373, w <i>R</i> <sub>2</sub> = 0.1008
<i>R</i> indices (all data)	<i>R</i> <sub>1</sub> = 0.0377, w <i>R</i> <sub>2</sub> = 0.1012
Absolute structure parameter	0.006(12)
Largest diff. peak and hole	0.944 and -0.596 e.Å <sup>-3</sup>

**Table S5.** Selected bond distances ( $\text{\AA}$ ) and bond angles ( $^\circ$ ) for the complex  $[\mathbf{L2}\text{Er}(\text{hfa})_3]$ .

Bond Distances / $\text{\AA}$					
Atom	Atom	Length/ $\text{\AA}$	Atom	Atom	Length/ $\text{\AA}$
Er(1)	O(1)	2.358(4)	Er(1)	O(6)	2.326(4)
Er(1)	O(2)	2.438(5)	Er(1)	N(1)	2.477(5)
Er(1)	O(3)	2.356(5)	Er(1)	N(3)	2.506(5)
Er(1)	O(4)	2.455(5)	Er(1)	N(4)	2.467(5)
Er(1)	O(5)	2.314(4)			
Bond Angles ( $^\circ$ )					
Atom	Atom	Atom	Angle / $^\circ$		
O(1)	Er(1)	O(2)	69.32(16)		
O(1)	Er(1)	O(4)	129.43(17)		
O(1)	Er(1)	N(1)	67.95(17)		
O(1)	Er(1)	N(3)	70.07(17)		
O(1)	Er(1)	N(4)	95.09(17)		
O(2)	Er(1)	O(4)	128.12(16)		
O(2)	Er(1)	N(1)	133.49(17)		
O(2)	Er(1)	N(3)	114.91(19)		
O(2)	Er(1)	N(4)	70.37(17)		
O(3)	Er(1)	O(1)	138.56(16)		
O(3)	Er(1)	O(2)	133.44(18)		
O(3)	Er(1)	O(4)	69.35(18)		
O(3)	Er(1)	N(1)	91.68(19)		
O(3)	Er(1)	N(3)	68.64(19)		
O(3)	Er(1)	N(4)	70.63(19)		
O(4)	Er(1)	N(1)	71.10(17)		
O(4)	Er(1)	N(3)	116.97(19)		
O(4)	Er(1)	N(4)	134.58(17)		
O(5)	Er(1)	O(1)	139.75(17)		
O(5)	Er(1)	O(2)	71.72(18)		
O(5)	Er(1)	O(3)	77.99(18)		
O(5)	Er(1)	O(4)	70.53(16)		
O(5)	Er(1)	O(6)	77.15(16)		
O(5)	Er(1)	N(1)	141.48(17)		
O(5)	Er(1)	N(3)	138.34(16)		
O(5)	Er(1)	N(4)	81.00(16)		
O(6)	Er(1)	O(1)	79.91(17)		
O(6)	Er(1)	O(2)	69.01(16)		

O(6)	Er(1)	O(3)	136.48(19)
O(6)	Er(1)	O(4)	68.90(18)
O(6)	Er(1)	N(1)	86.19(16)
O(6)	Er(1)	N(3)	144.51(16)
O(6)	Er(1)	N(4)	138.12(17)
N(1)	Er(1)	N(3)	65.53(17)
N(4)	Er(1)	N(1)	130.64(18)
N(4)	Er(1)	N(3)	65.12(17)

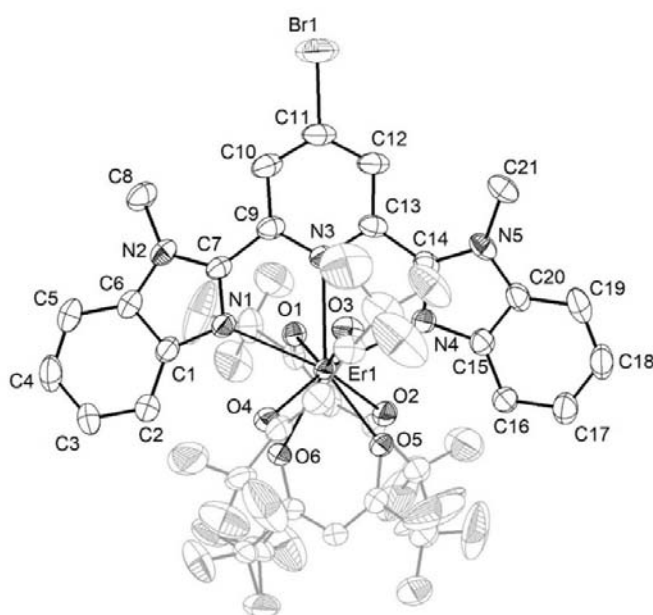


**Figure S2.** Ortep view of  $[L_2\text{Er}(\text{hfa})_3]$  (thermal ellipsoids are drawn at 50% probability level)

with numbering scheme. Hydrogen atoms and solvent molecules are omitted for clarity.

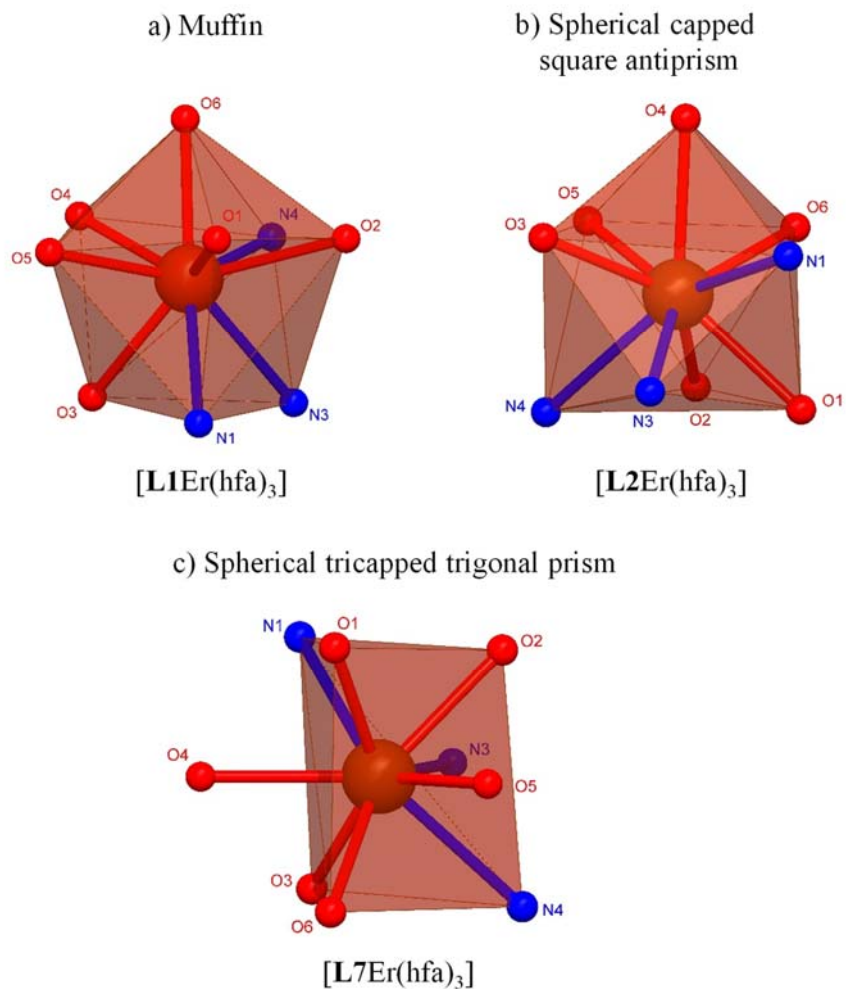


**Figure S3.** The three idealized coordination geometries deduced to display minimal distortions according to the Shape's analyses of the crystal structures (see Figure 2b and Table S6). For the SHAPE program, see D. Casanova, J. Cirera, M. Llunell, P. Alemany, D. Avnir, S. Alvarez, *J. Am. Chem. Soc.* **2004**, *126*, 1755-1763; S. Alvarez, *Dalton Trans.* **2005**, 2209-2233; E. Cremades, J. Echeverria, S. Alvarez, *Chem. Eur. J.* **2010**, *16*, 10380-10396.

**Table S6.** Deviation from the ideal possible shape calculated by program Shape 2.1<sup>[a]</sup> for complexes  $[\text{L}_k\text{Ln}(\text{hfa})_3]$ .

Shape	Ideal Point group	<b>[L1Er(hfa)<sub>3</sub>]</b>	<b>[L2Er(hfa)<sub>3</sub>]</b>	<b>[L3Eu(hfa)<sub>3</sub>]</b>	<b>[L4Eu(hfa)<sub>3</sub>]</b>	<b>[L5Eu(hfa)<sub>3</sub>]</b>	<b>[L6Eu(hfa)<sub>3</sub>]</b>	<b>[L7Er(hfa)<sub>3</sub>]</b>	<b>[L9Er(hfa)<sub>3</sub>]</b>
Enneagon	$D_{9h}$	36.395	35.784	35.820	35.625	35.989	35.624	37.200	35.442
Octagonal pyramid	$C_{8v}$	21.957	22.011	21.119	21.152	21.239	21.665	22.210	21.465
Heptagonal bipyramid	$D_{7h}$	17.707	18.900	17.708	16.862	16.943	16.236	20.600	17.688
Triangular cupola (J3)	$C_{3v}$	16.138	15.732	15.585	15.064	15.440	15.77	16.308	14.701
Capped cube J8	$C_{4v}$	10.294	10.290	9.443	9.158	9.371	10.216	10.961	9.958
Spherical-relaxed capped cube	$C_{4v}$	9.074	9.129	8.073	7.734	7.925	8.872	9.835	8.808
Capped square antiprism J10	$C_{4v}$	1.803	1.730	2.081	2.270	2.186	2.143	1.776	1.659
Spherical capped square antiprism	$C_{4v}$	<b>0.935</b>	<b>0.819</b>	1.194	1.358	1.216	1.086	0.807	<b>0.765</b>
Tricapped trigonal prism J51	$D_{3h}$	2.476	2.063	3.525	3.721	3.602	3.147	2.273	2.275
Spherical tricapped trigonal prism	$D_{3h}$	1.194	1.088	2.109	2.321	2.247	1.869	<b>0.515</b>	1.388
Tridiminished icosahedron J63	$C_{3v}$	12.711	13.396	11.695	11.887	12.184	12.814	13.083	12.531
Hula-hoop	$C_{2v}$	11.297	11.429	9.842	9.520	9.669	10.105	12.781	10.973
Muffin	$C_s$	<b>0.949</b>	0.996	<b>0.886</b>	<b>0.972</b>	<b>0.876</b>	<b>1.072</b>	1.513	0.913

<sup>[a]</sup>D. Casanova, J. Cirera, M. Llunell, P. Alemany, D. Avnir, S. Alvarez, *J. Am. Chem. Soc.* **2004**, *126*, 1755-1763; S. Alvarez, *Dalton Trans.* **2005**, 2209-2233; E. Cremades, J. Echeverria, S. Alvarez, *Chem. Eur. J.* **2010**, *16*, 10380-10396.

**Table S7.** Bond valences ( $\nu_{\text{Ln},j}$ ), average bond valences ( $\bar{\nu}_{\text{Ln},j}$ ) and bond valence sums ( $V_{\text{Ln},j}$ ) in the crystal structures of  $[\text{L}k\text{Eu(hfa)}_3]$  were calculated using  $R_{ij}$  values for 9 coordinated compounds and eq (A1-2).<sup>[a]</sup>

Atoms	$[\text{L1}\text{Eu(hfa)}_3]$ <sup>[67]</sup>		$[\text{L2}\text{Eu(hfa)}_3]$		$[\text{L3}\text{Eu(hfa)}_3]$ <sup>[66]</sup>		$[\text{L4}\text{Eu(hfa)}_3]$ <sup>[66]</sup>		$[\text{L5}\text{Eu(hfa)}_3]$ <sup>[66]</sup>	
	$R_{\text{Eu}}^{\text{CN}=9} = 1.120 \text{ \AA}$ <sup>[b]</sup>									
$\nu_{\text{Eu},j}$	$(\bar{\nu}_{\text{Eu},j})$	$\nu_{\text{Eu},j}$								
Eu-N(1) (Bz1)	0.354(6)	0.337(22)	0.394(12)	0.357(39)	0.373(6)	0.345(51)	0.342(6)	0.326(49)	0.344(5)	0.324(32)
Eu-N(2) (Py)	0.312(5)		0.316(9)		0.287(5)		0.271(5)		0.287(5)	
Eu-N(3) (Bz2)	0.345(6)		0.360(11)		0.376(6)		0.364(7)		0.340(5)	
Eu-O(1) (hfa1)	0.352(14)	0.355(43)	0.344(16)	0.358(39)	0.357(14)	0.355(31)	0.357(14)	0.354(26)	0.357(14)	0.362(25)
Eu-O(2) (hfa1)	0.304(12)		0.300(14)		0.309(12)		0.321(13)		0.328(13)	
Eu-O(3) (hfa2)	0.407(16)		0.421(18)		0.399(15)		0.399(16)		0.401(15)	
Eu-O(4) (hfa2)	0.403(16)		0.380(17)		0.377(14)		0.363(14)		0.376(15)	
Eu-O(5) (hfa3)	0.316(12)		0.317(15)		0.336(13)		0.344(14)		0.356(14)	
Eu-O(6) (hfa3)	0.349(14)		0.386(17)		0.354(14)		0.342(13)		0.350(13)	
$V_{\text{Ln},j}$	3.143(35)		3.218(44)		3.168(35)		3.102(36)		3.140(35)	

<sup>[a]</sup> Bond valence parameters are taken from A. Trzesowska, R. Kruszynski, T. J. Bartczak, *Acta Cryst B Structural Science* **2004**, *B60*, 174-178 for Ln-O bonds and A. Trzesowska, R. Kruszynski, T. J. Bartczak, *Acta Cryst B Structural Science* **2005**, *B61*, 429-434 for Ln-N bonds. <sup>[b]</sup>Nine-coordinate ionic radii taken from R. D. Shannon, *Acta Crystallogr., Sect. A* **1976**, *32*, 751-767 revised by P. D'Angelo, A. Zitolo, V. Migliorati, G. Chillemi, M. Duvail, P. Vitorge, S. Abadie, R. Spezia, *Inorg. Chem.* **2011**, *50*, 4572-4579.

**Table S7.** Continued.

Atoms	[L6Eu(hfa)3] <sup>[67]</sup> $R_{\text{Eu}}^{\text{CN}=9} = 1.120 \text{ \AA}^{[\text{b}]}$		[L7Eu(hfa)3] <sup>[67]</sup> $R_{\text{Eu}}^{\text{CN}=9} = 1.120 \text{ \AA}^{[\text{b}]}$		[L9Eu(hfa)3] <sup>[68]</sup> $R_{\text{Eu}}^{\text{CN}=9} = 1.120 \text{ \AA}^{[\text{b}]}$	
	$\nu_{\text{Eu},j}$	$(\bar{\nu}_{\text{Eu},j})$	$\nu_{\text{Eu},j}$	$(\bar{\nu}_{\text{Eu},j})$	$\nu_{\text{Eu},j}$	$(\bar{\nu}_{\text{Eu},j})$
Eu-N(1) (Bz1)	0.259(4)	0.276(24)	0.258(4)	0.275(40)	0.353(6)	0.321(42)
Eu-N(2) (Py)	0.303(5)		0.321(5)		0.273(4)	
Eu-N(3) (Bz2)	0.266(4)		0.246(4)		0.336(5)	
Eu-O(1) (hfa1)	0.343(13)	0.373(31)	0.394(15)	0.364(21)	0.369(14)	0.358(42)
Eu-O(2) (hfa1)	0.377(15)		0.354(13)		0.319(12)	
Eu-O(3) (hfa2)	0.394(15)		0.351(13)		0.411(16)	
Eu-O(4) (hfa2)	0.396(15)		0.377(14)		0.399(15)	
Eu-O(5) (hfa3)	0.326(13)		0.335(13)		0.307(12)	
Eu-O(6) (hfa3)	0.401(16)		0.372(14)		0.346(13)	
$V_{\text{Ln},j}$	3.064(36)		3.009(35)		3.112(35)	

<sup>[a]</sup>Bond valence parameters are taken from A. Trzesowska, R. Kruszynski, T. J. Bartczak, *Acta Cryst B Structural Science* **2004**, *B60*, 174-178 for Ln-O bonds and A. Trzesowska, R. Kruszynski, T. J. Bartczak, *Acta Cryst B Structural Science* **2005**, *B61*, 429-434 for Ln-N bonds. <sup>[b]</sup>Nine-coordinate ionic radii taken from R. D. Shannon, *Acta Crystallogr., Sect. A* **1976**, *32*, 751-767 revised by P. D'Angelo, A. Zitolo, V. Migliorati, G. Chillemi, M. Duvail, P. Vitorge, S. Abadie, R. Spezia, *Inorg. Chem.* **2011**, *50*, 4572-4579.

**Table S8.** Bond valences ( $\nu_{\text{Ln},j}$ ), average bond valences ( $\bar{\nu}_{\text{Ln},j}$ ) and bond valence sums ( $V_{\text{Ln},j}$ ) in the crystal structures of  $[\text{LkEr(hfa)}_3]$  were calculated using  $R_{ij}$  values for 9 coordinated compounds and eq (A1-2).<sup>[a]</sup>

Atoms	$[\text{L1Er(hfa)}_3]$ <sup>[67]</sup> $R_{\text{Er}}^{\text{CN}=9} = 1.062 \text{ \AA}$ <sup>[b]</sup>		$[\text{L2Er(hfa)}_3]$ $R_{\text{Er}}^{\text{CN}=9} = 1.062 \text{ \AA}$ <sup>[b]</sup>		$[\text{L7Er(hfa)}_3]$ <sup>[67]</sup> $R_{\text{Er}}^{\text{CN}=9} = 1.062 \text{ \AA}$ <sup>[b]</sup>		$[\text{L9Er(hfa)}_3]$ <sup>[68]</sup> $R_{\text{Er}}^{\text{CN}=9} = 1.062 \text{ \AA}$ <sup>[b]</sup>	
	$\nu_{\text{Er},j}$	$(\bar{\nu}_{\text{Er},j})$	$\nu_{\text{Er},j}$	$(\bar{\nu}_{\text{Er},j})$	$\nu_{\text{Er},j}$	$(\bar{\nu}_{\text{Er},j})$	$\nu_{\text{Eu},j}$	$(\bar{\nu}_{\text{Eu},j})$
Er-N(1) (Bz1)	0.342(15)	0.333(12)	0.362(16)	0.356(19)	0.239(11)	0.268(44)	0.342(6)	0.326(49)
Er-N(2) (Py)	0.319(14)		0.335(15)		0.318(14)		0.271(5)	
Er-N(3) (Bz2)	0.338(15)		0.372(17)		0.246(11)		0.364(7)	
Er-O(1) (hfa1)	0.276(11)	0.349(55)	0.361(14)	0.349(53)	0.379(15)	0.364(25)	0.357(14)	0.354(26)
Er-O(2) (hfa1)	0.356(14)		0.291(12)		0.359(14)		0.321(13)	
Er-O(3) (hfa2)	0.351(13)		0.363(15)		0.397(15)		0.399(16)	
Er-O(4) (hfa2)	0.297(11)		0.278(11)		0.340(13)		0.363(14)	
Er-O(5) (hfa3)	0.407(16)		0.407(16)		0.331(13)		0.344(14)	
Er-O(6) (hfa3)	0.409(16)		0.394(15)		0.379(15)		0.342(13)	
$V_{\text{Ln},j}$	3.095(42)		3.161(40)		2.988(40)		3.102(36)	

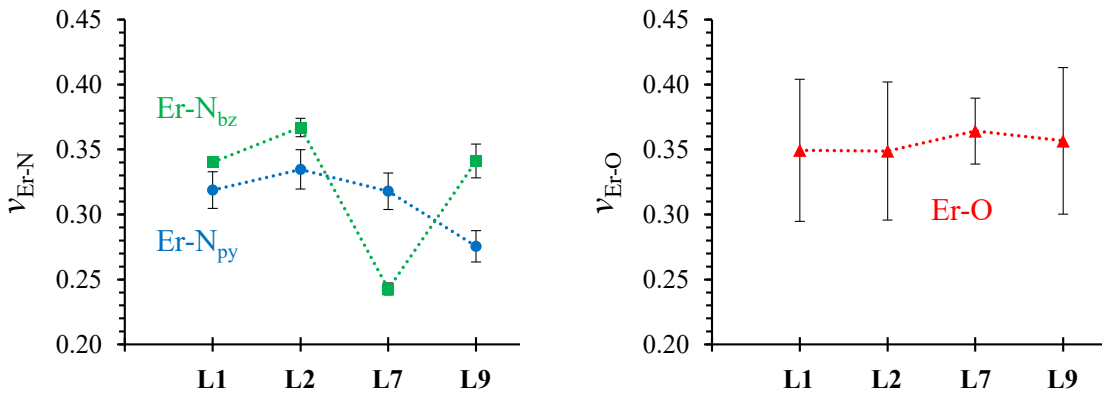
<sup>[a]</sup>Bond valence parameters are taken from A. Trzesowska, R. Kruszynski, T. J. Bartczak, *Acta Cryst B Structural Science* **2004**, *B60*, 174-178 for Ln-O bonds and A. Trzesowska, R. Kruszynski, T. J. Bartczak, *Acta Cryst B Structural Science* **2005**, *B61*, 429-434 for Ln-N bonds. <sup>[b]</sup>Nine-coordinate ionic radii taken from R. D. Shannon, *Acta Crystallogr., Sect. A* **1976**, *32*, 751-767 revised by P. D'Angelo, A. Zitolo, V. Migliorati, G. Chillemi, M. Duvail, P. Vitorge, S. Abadie, R. Spezia, *Inorg. Chem.* **2011**, *50*, 4572-4579.

**Table S9.** Bond valences ( $\nu_{\text{Ln},j}$ ), average bond valences ( $\bar{\nu}_{\text{Ln},j}$ ) and bond valence sums ( $V_{\text{Ln},j}$ ) in the crystal structures of  $[\text{LkLa(hfa)}_3]$  were calculated using  $R_{ij}$  values for 9 coordinated compounds and eq (A1-2).<sup>[a]</sup>

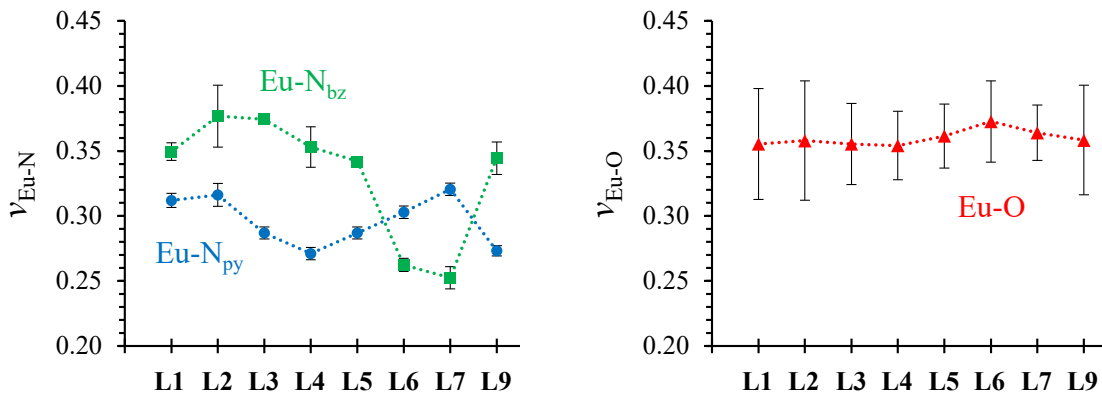
Atoms	$[\text{L1La(hfa)}_3]$ <sup>[67]</sup> $R_{\text{La}}^{\text{CN}=9} = 1.216 \text{ \AA}$ <sup>[b]</sup>		$[\text{L3La(hfa)}_3]$ <sup>[66]</sup> $R_{\text{La}}^{\text{CN}=9} = 1.216 \text{ \AA}$ <sup>[b]</sup>		$[\text{L7La(hfa)}_3]$ <sup>[66]</sup> $R_{\text{La}}^{\text{CN}=9} = 1.216 \text{ \AA}$ <sup>[b]</sup>		$[\text{L9La(hfa)}_3]$ <sup>[68]</sup> $R_{\text{La}}^{\text{CN}=9} = 1.216 \text{ \AA}$ <sup>[b]</sup>	
	$\nu_{\text{La},j}$	$(\bar{\nu}_{\text{La},j})$	$\nu_{\text{La},j}$	$(\bar{\nu}_{\text{La},j})$	$\nu_{\text{La},j}$	$(\bar{\nu}_{\text{La},j})$	$\nu_{\text{La},j}$	$(\bar{\nu}_{\text{La},j})$
Er-N(1) (Bz1)	0.364(12)	0.340(32)	0.381(12)	0.324(64)	0.278(9)	0.285(28)	0.357(11)	0.306(65)
Er-N(2) (Py)	0.303(10)		0.255(8)		0.316(10)		0.233(7)	
Er-N(3) (Bz2)	0.352(12)		0.335(10)		0.262(8)		0.327(10)	
Er-O(1) (hfa1)	0.365(21)	0.367(33)	0.310(18)	0.354(25)	0.375(21)	0.366(15)	0.371(21)	0.364(23)
Er-O(2) (hfa1)	0.327(19)		0.380(22)		0.382(22)		0.363(21)	
Er-O(3) (hfa2)	0.405(23)		0.345(20)		0.350(20)		0.325(19)	
Er-O(4) (hfa2)	0.404(23)		0.374(21)		0.381(22)		0.389(22)	
Er-O(5) (hfa3)	0.337(20)		0.350(20)		0.354(20)		0.352(20)	
Er-O(6) (hfa3)	0.362(21)		0.366(21)		0.355(20)		0.381(22)	
$V_{\text{Ln},j}$	3.220(56)		3.096(53)		3.054(54)		3.098(53)	

<sup>[a]</sup>Bond valence parameters are taken from A. Trzesowska, R. Kruszynski, T. J. Bartczak, *Acta Cryst B Structural Science* **2004**, *B60*, 174-178 for Ln-O bonds and A. Trzesowska, R. Kruszynski, T. J. Bartczak, *Acta Cryst B Structural Science* **2005**, *B61*, 429-434 for Ln-N bonds. <sup>[b]</sup>Nine-coordinate ionic radii taken from R. D. Shannon, *Acta Crystallogr., Sect. A* **1976**, *32*, 751-767 revised by P. D'Angelo, A. Zitolo, V. Migliorati, G. Chillemi, M. Duvail, P. Vitorge, S. Abadie, R. Spezia, *Inorg. Chem.* **2011**, *50*, 4572-4579.

a)  $[\mathbf{Lk}\text{Er}(\text{hfa})_3]$



b)  $[\mathbf{Lk}\text{Eu}(\text{hfa})_3]$



c)  $[\mathbf{Lk}\text{La}(\text{hfa})_3]$

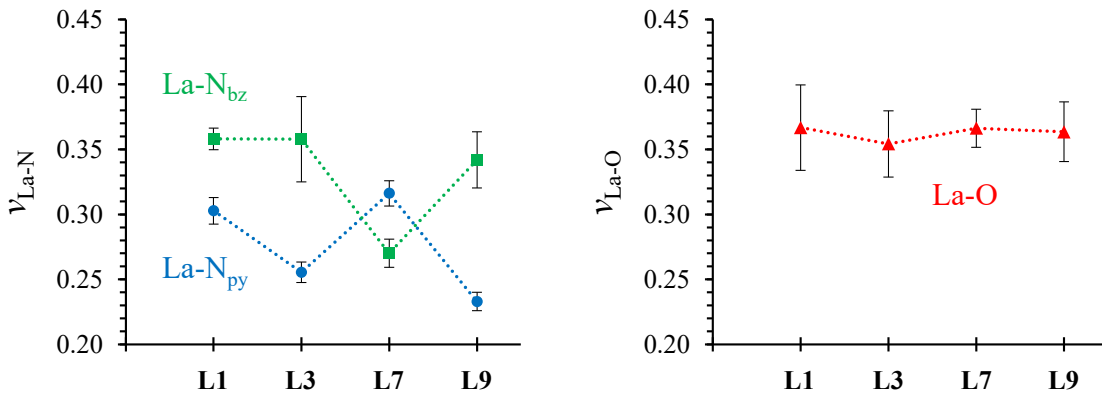


**Figure S4.** Average  $v_{\text{Er}-\text{Nbenzimidazole}}$  (green),  $v_{\text{Er}-\text{Npyridine}}$  (blue), and average  $v_{\text{Er}-\text{O(hfa)}}$  (red) bond valences calculated with eq (A1-2) for the molecular structures of complexes a)  $[\mathbf{Lk}\text{Er}(\text{hfa})_3]$ , b)  $[\mathbf{Lk}\text{Eu}(\text{hfa})_3]$  and c)  $[\mathbf{Lk}\text{La}(\text{hfa})_3]$  in their crystalline state. Standard deviations of the average are shown with vertical error bars. The dashed linear traces are only guides for the eyes.

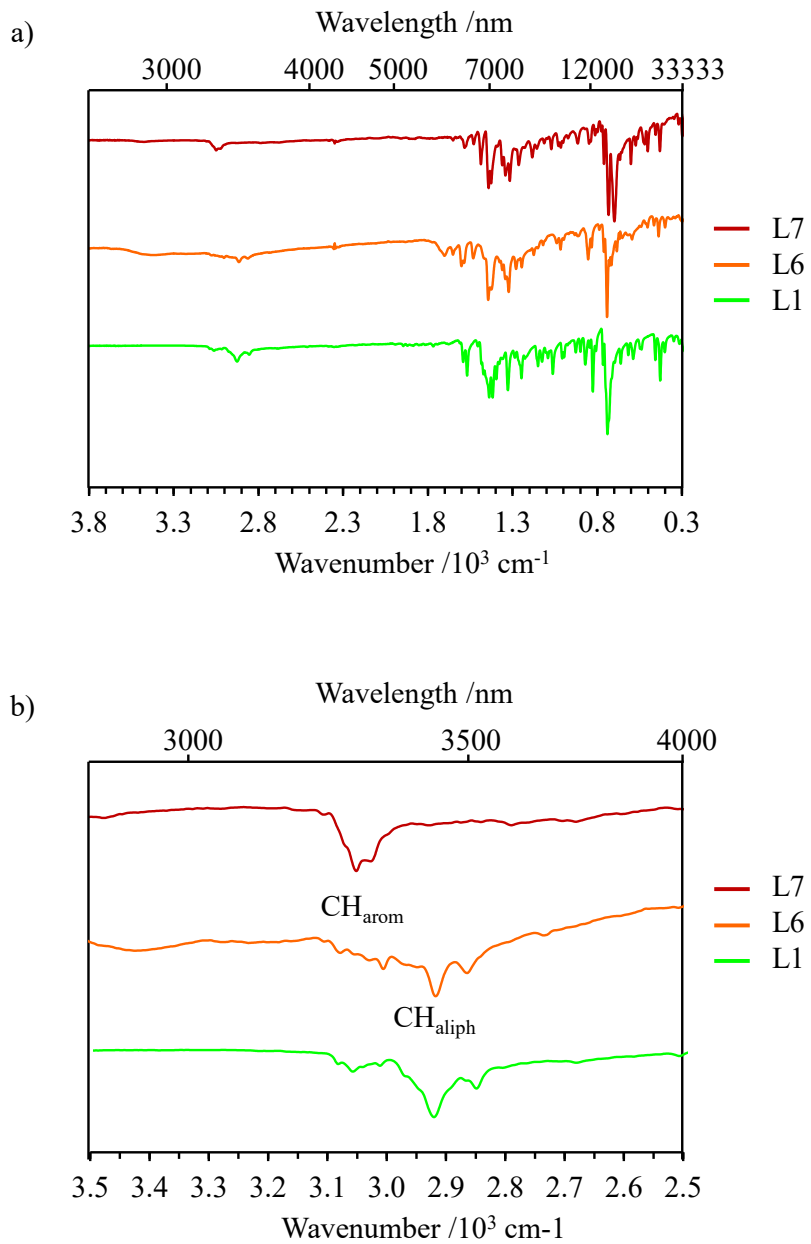


**Figure S5.** a) Infrared spectra of ligands **L1**, **L6** and **L7** recorded in the solid state at 293 K. b) Highlight of the CH stretching domain.

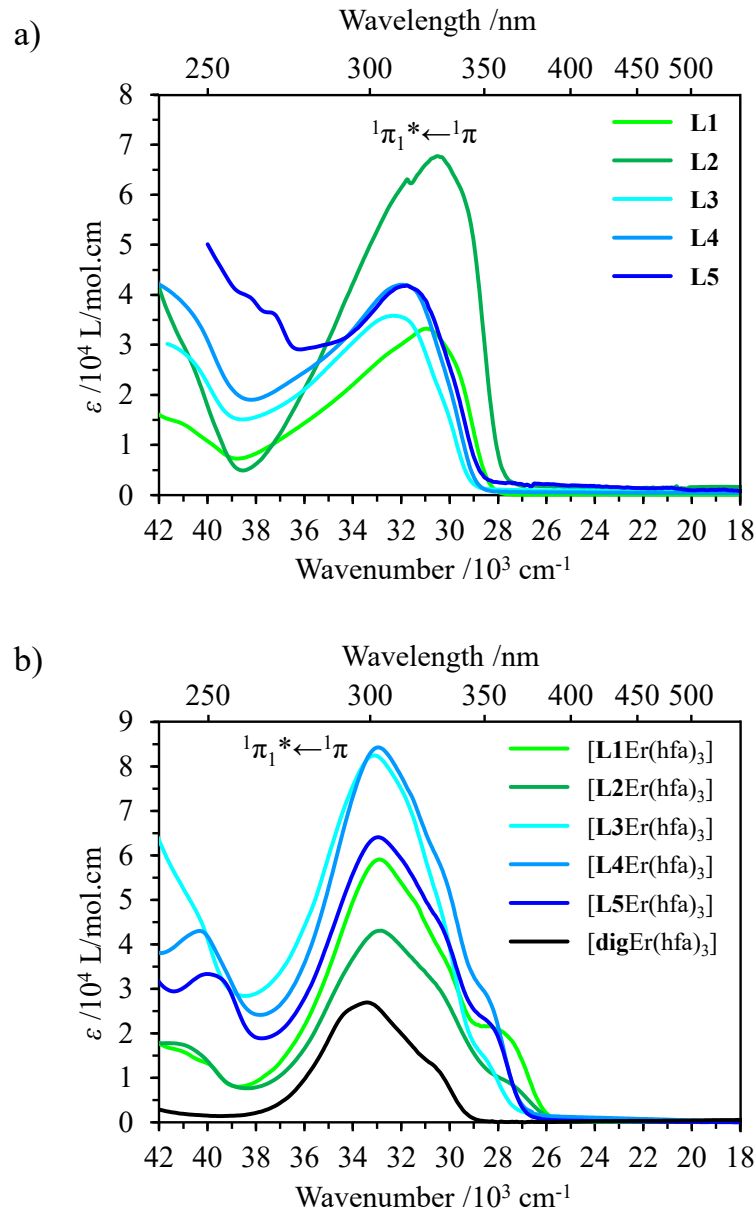


**Figure S6.** UV-Vis absorption spectra of a) ligands **L1-L5** and b) their corresponding  $[\mathbf{L}k\text{Er}(\text{hfa})_3]$  complexes recorded in  $\text{CH}_2\text{Cl}_2$  solution ( $5 \times 10^{-6} \text{ M}$ ) in a 1.0 cm cuvette at 293 K.

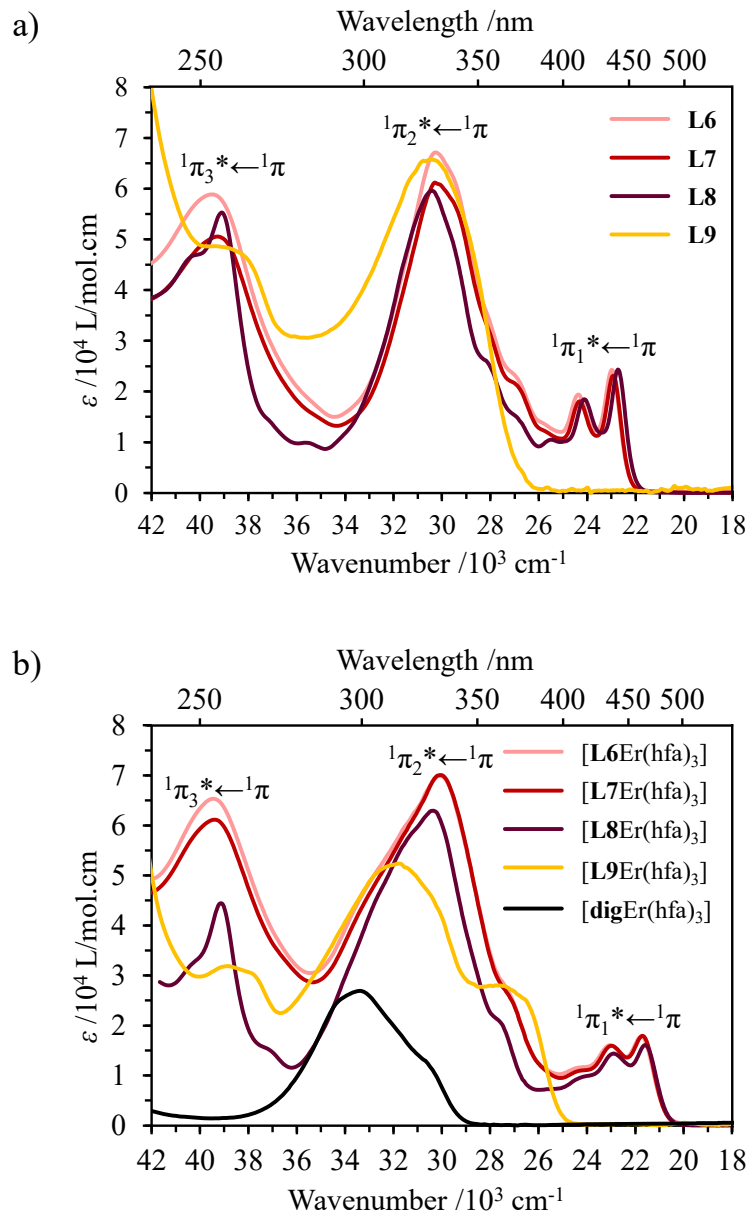


**Figure S7.** UV-Vis absorption spectra of a) ligands L6-L9 and b) their corresponding  $[\text{L}k\text{Er}(\text{hfa})_3]$  complexes recorded in  $\text{CH}_2\text{Cl}_2$  solution ( $5 \times 10^{-6}$  M) in a 1.0 cm cuvette at 293 K.

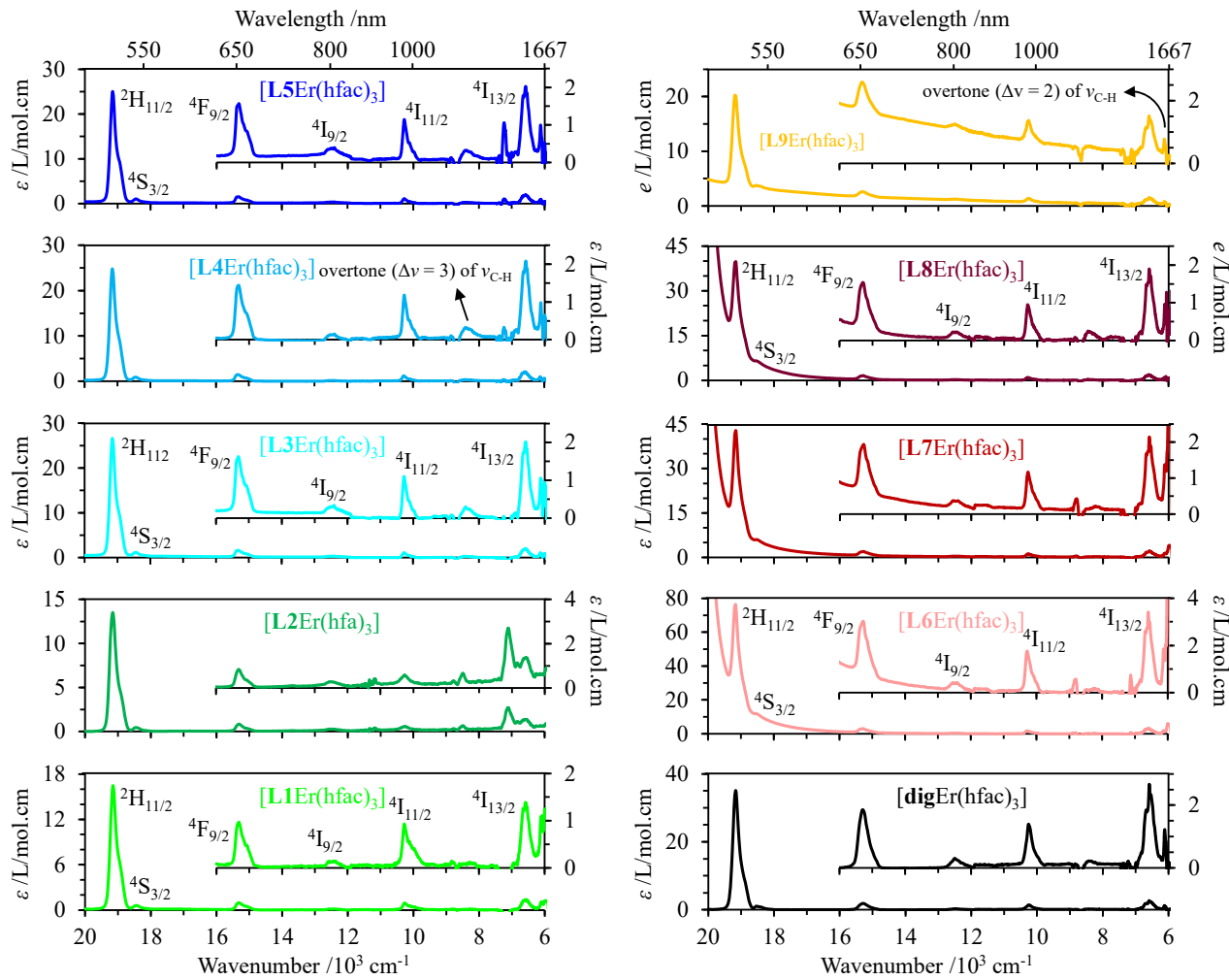


**Figure S8.** Visible to near-infrared absorption spectra of  $[\text{L}k\text{Er}(\text{hfa})_3]$  complexes recorded in  $\text{CH}_2\text{Cl}_2$  solution (5–10 mM) and in acetonitrile (10 mM) for  $[\text{L}2\text{Er}(\text{hfa})_3]$  in 1.0 cm cuvettes at 293 K. The Er-centered  $^{2S+1}\text{L}_J \leftarrow ^4\text{I}_{15/2}$  transitions are assigned.

**Table S10.** Radiative lifetimes for the Er( $^{2S+1}L_J \rightarrow ^4I_{15/2}$ ) transitions calculated using

$$\frac{1}{\tau_{rad}} = 2303 \times \frac{8\pi cn^2 \tilde{v}_m^2 (2J+1)}{N_A (2J'+1)} \int \mathcal{E}(\tilde{\nu}) d\tilde{\nu} \quad (\text{eq 3})$$

(eq 3) for selected Er(III) excited levels in [Er(Et-bzimpy)<sub>3</sub>]<sup>3+</sup>

(CH<sub>3</sub>CN solution), [**dig**Er(hfa)<sub>3</sub>], and [**Lk**Er(hfa)<sub>3</sub>] complexes in CH<sub>2</sub>Cl<sub>2</sub> solution at 293 K.<sup>[a]</sup>

Compound <sup>[b]</sup>	$\tau_{\text{Er,rad}}^{^4\text{I}_{13/2}}$ /ms	$\tau_{\text{Er,rad}}^{^4\text{I}_{11/2}}$ /ms	$\tau_{\text{Er,rad}}^{^2\text{I}_{9/2}}$ /ms	$\tau_{\text{Er,rad}}^{^4\text{F}_{9/2}}$ /ms	$\tau_{\text{Er,rad}}^{^4\text{S}_{3/2}}$ /ms	$\tau_{\text{Er,rad}}^{^2\text{H}_{11/2}}$ /ms
[Er(Et-bzimpy) <sub>3</sub> ] <sup>3+</sup>	7.12(5)	15(1)	15(1)	1.6(1)	1.31(9)	4.6(3)·10 <sup>-1</sup>
[ <b>dig</b> Er(hfa) <sub>3</sub> ]	5.0(2)	3.8(2)	5.8(3)	0.65(3)	0.51(2)	3.5(2)·10 <sup>-2</sup>
[ <b>L1</b> Er(hfa) <sub>3</sub> ]	6.4(3)	5.0(2)	7.5(3)	1.07(5)	0.89(4)	5.5(2)·10 <sup>-2</sup>
[ <b>L2</b> Er(hfa) <sub>3</sub> ]	3.5(2)	9.4(4)	6.8(3)	2.10(9)	1.85(8)	9.9(4)·10 <sup>-2</sup>
[ <b>L3</b> Er(hfa) <sub>3</sub> ]	6.6(3)	4.7(2)	9.3(4)	0.93(4)	0.73(3)	5.0(2)·10 <sup>-2</sup>
[ <b>L4</b> Er(hfa) <sub>3</sub> ]	6.2(3)	5.1(2)	9.5(4)	0.92(4)	0.95(4)	5.0(2)·10 <sup>-2</sup>
[ <b>L5</b> Er(hfa) <sub>3</sub> ]	6.5(3)	4.9(2)	8.9(4)	0.95(4)	0.96(4)	5.4(2)·10 <sup>-2</sup>
[ <b>L6</b> Er(hfa) <sub>3</sub> ]	4.7(2)	3.3(1)	7.8(4)	0.66(3)	0.32(1)	2.2(1)·10 <sup>-2</sup>
[ <b>L7</b> Er(hfa) <sub>3</sub> ]	7.9(4)	4.8(2)	10.7(5)	0.97(4)	0.64(3)	3.7(2)·10 <sup>-2</sup>
[ <b>L8</b> Er(hfa) <sub>3</sub> ]	7.5(3)	4.5(2)	11.6(5)	1.05(5)	0.69(3)	4.1(2)·10 <sup>-2</sup>
[ <b>L9</b> Er(hfa) <sub>3</sub> ]	12.6(6)	5.3(2)	12.0(5)	1.26(6)	1.10(5)	7.6(3)·10 <sup>-2</sup>

<sup>[a]</sup>For the solution samples ( $c = 5\text{-}10 \text{ mM}$ ),  $\tau_{\text{Er,rad}}$  was calculated with the refractive index  $n_{\text{DCM}} = 1.424$ .<sup>[b]</sup>For the [**L2**Er(hfa)<sub>3</sub>] and [Er(Et-bzimpy)<sub>3</sub>]<sup>3+</sup> complexes the measurements were performedin CH<sub>3</sub>CN with  $n_{\text{acetonitrile}} = 1.344$ . Data for [Er(Et-bzimpy)<sub>3</sub>]<sup>3+</sup> were taken from Golesorkhi et. al.*Dalton Trans., 2021, 50, 7955-7968.*<sup>[59]</sup>

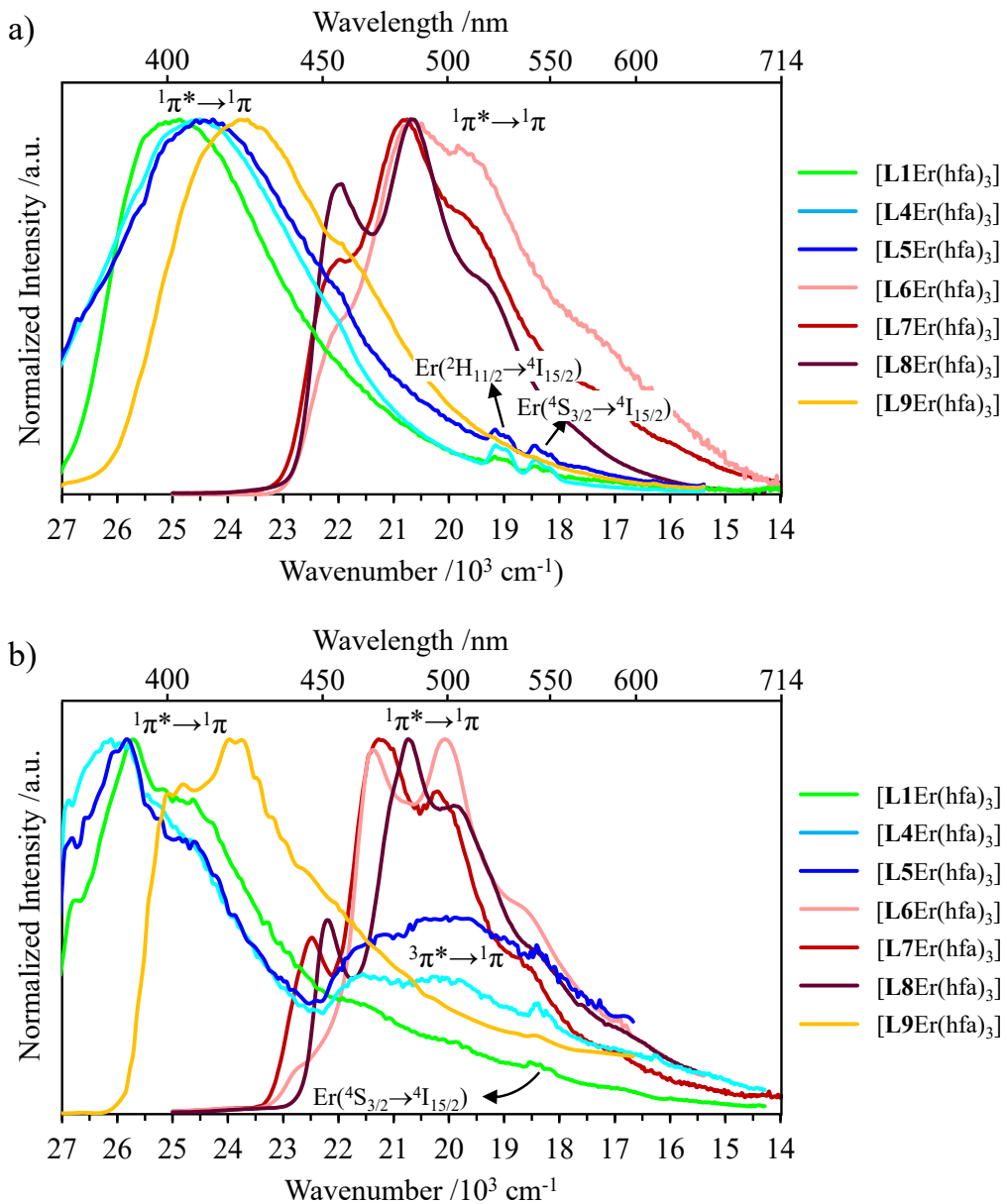


**Figure S9.** Normalized emission spectra of  $[Lk\text{Er}(\text{hfa})_3]$  ( $5 \times 10^{-6}$  M,  $\lambda_{\text{exc}} = 350$  nm) recorded in DCM solution at a) 293 K and b) 77 K.

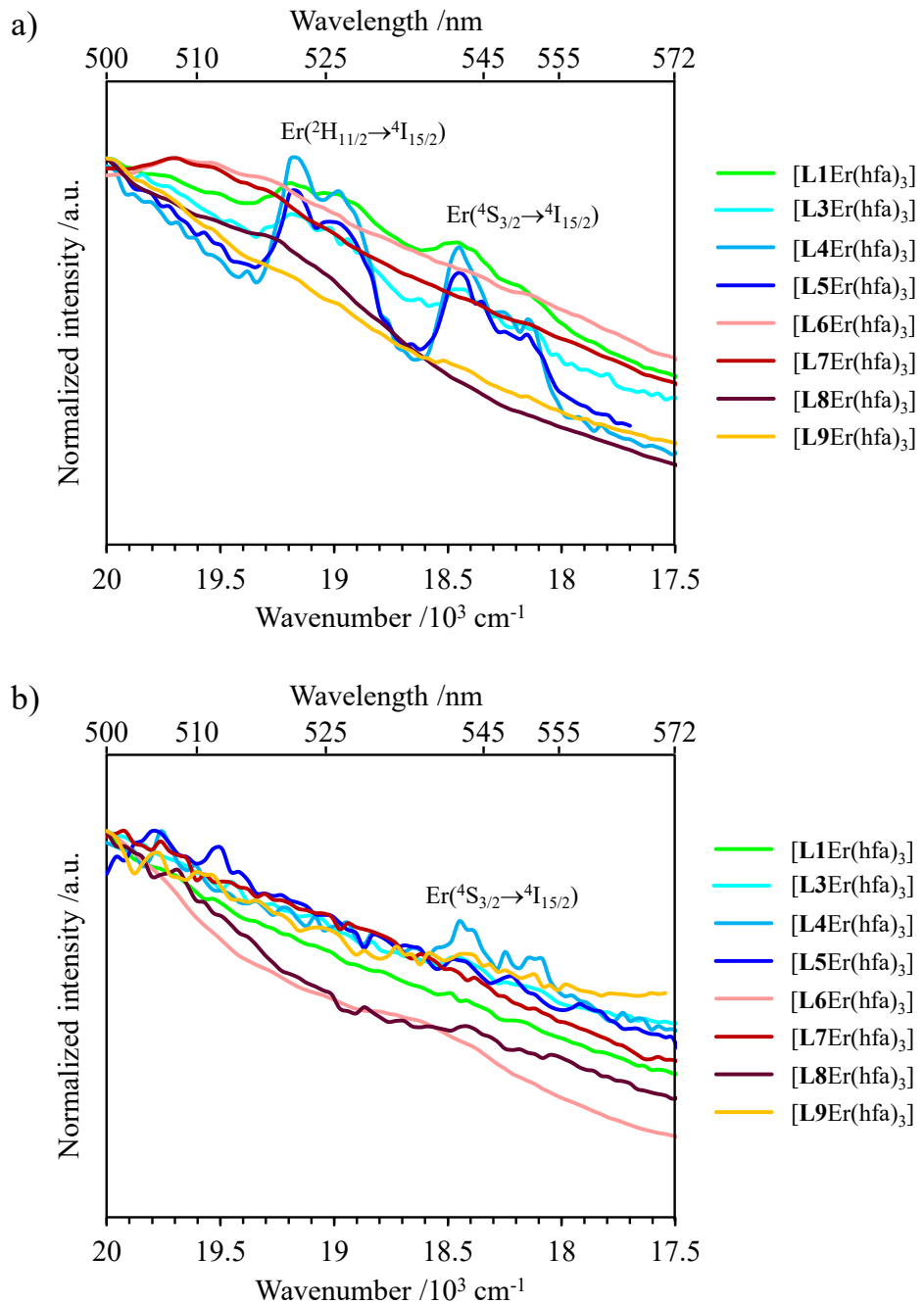


**Figure S10.** Spectral window of 500–580 nm for detecting the Er(III) visible emissions arising from ligand-to-metal energy transfer via the antenna effect ( $\lambda_{\text{exc}} = 350 \text{ nm}$ ) in DCM solution ( $C \approx 5 \times 10^{-6} \text{ M}$ ) recorded at a) room temperature and b) 77 K.

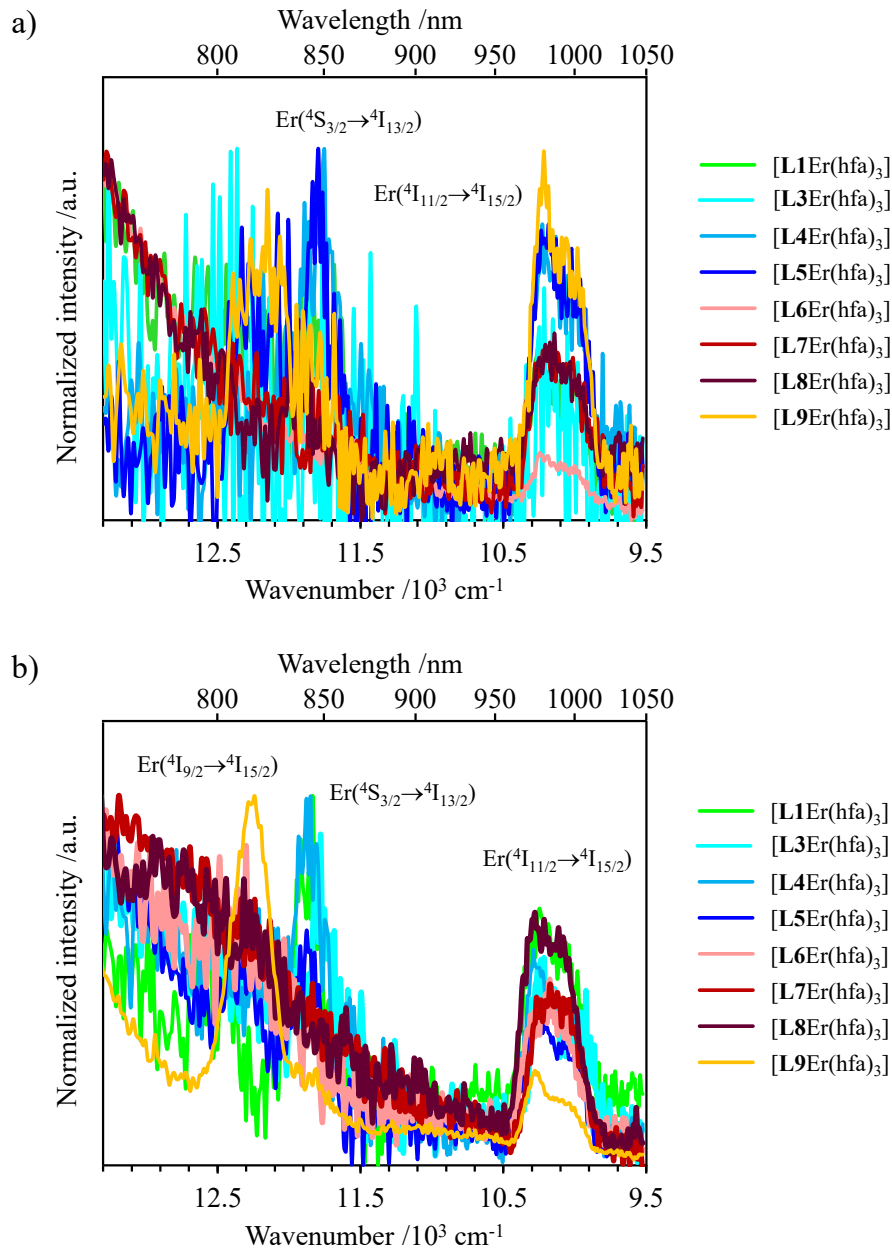


**Figure S11.** Normalised emission spectra ( $\lambda_{\text{exc}} = 350 \text{ nm}$ ) of the  $[\text{L}k\text{Er}(\text{hfa})_3]$  complexes in DCM solution ( $C \approx 5 \times 10^{-6} \text{ M}$ ) highlighting the spectral window associated with  $\text{Er}({}^4\text{I}_{9/2} \rightarrow {}^4\text{I}_{15/2})$ ,  $\text{Er}({}^4\text{I}_{11/2} \rightarrow {}^4\text{I}_{15/2})$ , and  $\text{Er}({}^4\text{S}_{3/2} \rightarrow {}^4\text{I}_{13/2})$  transitions at a) room temperature and b) 77 K.

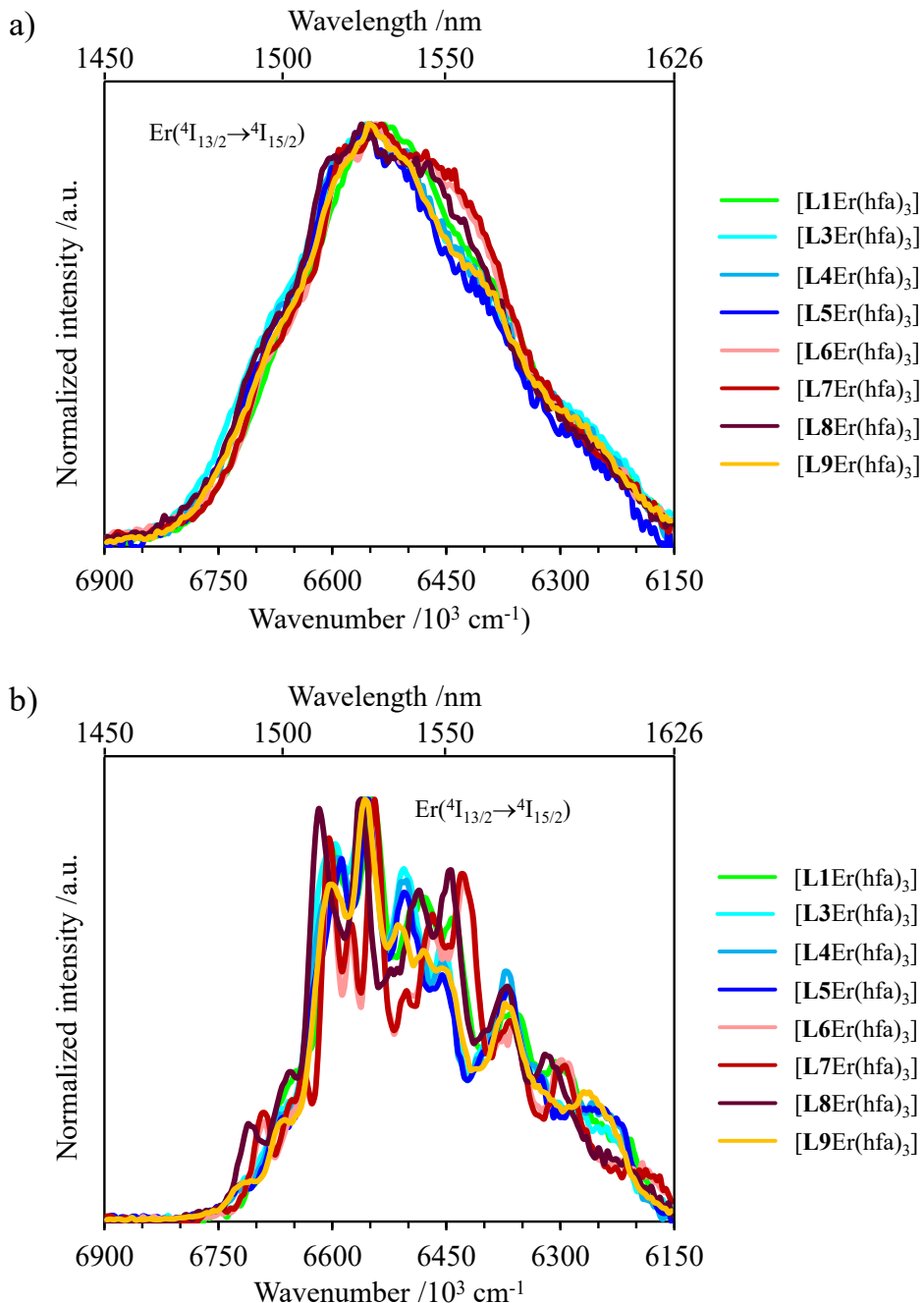


**Figure S12.** Normalised infra-red emission spectra ( $\lambda_{\text{exc}} = 350 \text{ nm}$ ) of the  $\text{Er}({}^4\text{I}_{13/2} \rightarrow {}^4\text{I}_{15/2})$  transition in  $[\text{L}k\text{Er}(\text{hfa})_3]$  complexes, following the antenna mechanism in DCM solution ( $C \approx 5 \times 10^{-6} \text{ M}$ ) recorded at a) room temperature and b) 77 K.

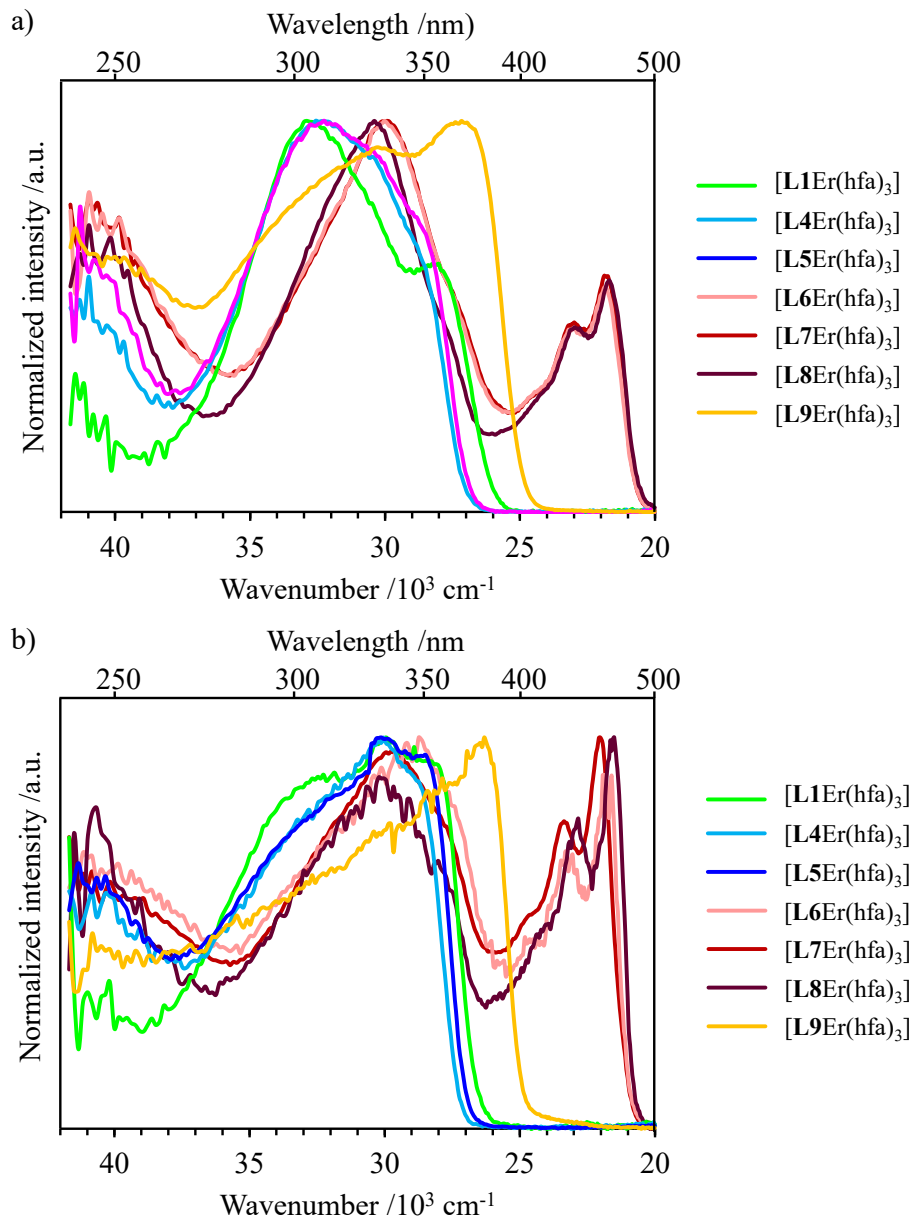


**Figure S13.** Normalized excitation spectra of DCM solution of  $[\text{L}k\text{Er}(\text{hfa})_3]$  complexes ( $\lambda_{\text{em}} = 1531$  nm,  $5 \times 10^{-6}$  M in DCM) recorded at a) 293 K and b) 77 K.

**Table S11.** Ground state absorption cross section ( $\sigma_{\text{Er}}^{0 \rightarrow 1} / \text{cm}^2$ ), rate constants ( $k_{\text{Er}}^{i \rightarrow j} / \text{s}^{-1}$ ), upconversion quantum yields ( $\phi_{\text{tot}}^{\text{up}}$ ,  $\lambda_{\text{exc}} = 801 \text{ nm}$ , and  $P = 25 \text{ W} \cdot \text{cm}^{-2}$ ) and ESA efficiency ( $\eta_{\text{ESA}}$ ,  $\lambda_{\text{exc}} = 801 \text{ nm}$ , and normalized at  $P = 25 \text{ W} \cdot \text{cm}^{-2}$ ) for  $[\text{LkEr(hfa)}_3]$  in DCM solution at 293 K. The excited state absorption cross sections ( $\sigma_{\text{Er}}^{1 \rightarrow 2} / \text{cm}^2$ ) are deduced by using the upconversion mechanism ③ depicted in Scheme 3.

Complexes	$\sigma_{\text{Er}}^{0 \rightarrow 1}$ [a]	$k_{\text{Er}}^{1 \rightarrow 0} / 10^5$ [b]	$k_{\text{Er}}^{2 \rightarrow 0} / 10^2$ [c]	$k_{\text{Er}}^{2 \rightarrow 1} / 10^7$ [d]	$\phi_{\text{tot}}^{\text{up}}$ [e]	$\eta_{\text{ESA}}$ [f]	$\sigma_{\text{Er}}^{1 \rightarrow 2}$ [a],[g]
$[\text{Er(Et-bzimpy)}_3]^{3+}$	$4.8(2) \cdot 10^{-22} [0.125(6)]$	$1.80(2)$	$7.6(5)$	$5.0(3)$	$1.7(2) \cdot 10^{-9}$	$1.1(2) \cdot 10^{-4}$	$2.0(3) \cdot 10^{-19} [52(8)]$
$[\text{L1Er(hfa)}_3]$	$6.3(3) \cdot 10^{-22} [0.165(8)]$	$3.50(4)$	$11.2(5)$	$29(2)$	$3.0(3) \cdot 10^{-7}$	$7.7(9) \cdot 10^{-2}$	$2.9(4) \cdot 10^{-16} [7.6(9) \cdot 10^4]$
$[\text{L2Er(hfa)}_3]$	$7.8(4) \cdot 10^{-22} [0.206(10)]$	$3.48(5)$	$5.4(2)$	$29(2)$	$1.1(1) \cdot 10^{-7}$	$5.8(7) \cdot 10^{-2}$	$2.1(3) \cdot 10^{-16} [5.6(7) \cdot 10^4]$
$[\text{L3Er(hfa)}_3]$	$1.06(5) \cdot 10^{-21} [0.280(14)]$	—	—	—	$3.0(3) \cdot 10^{-7}$	$6.2(7) \cdot 10^{-2}$	—
$[\text{L4Er(hfa)}_3]$	$5.4(3) \cdot 10^{-22} [0.142(7)]$	$3.53(4)$	$10.5(4)$	$29(2)$	$5.3(5) \cdot 10^{-8}$	$1.4(2) \cdot 10^{-2}$	$5.1(6) \cdot 10^{-17} [1.3(2) \cdot 10^4]$
$[\text{L5Er(hfa)}_3]$	$9.5(5) \cdot 10^{-22} [0.251(13)]$	$3.58(4)$	$10.4(4)$	$29(2)$	$1.0(1) \cdot 10^{-7}$	$2.8(3) \cdot 10^{-2}$	$1.0(1) \cdot 10^{-16} [2.6(3) \cdot 10^4]$
$[\text{L6Er(hfa)}_3]$	$1.14(6) \cdot 10^{-21} [0.301(15)]$	$3.19(5)$	$31.25(98)$	$29(2)$	$3.1(3) \cdot 10^{-7}$	$2.9(3) \cdot 10^{-2}$	$9(1) \cdot 10^{-17} [2.4(9) \cdot 10^4]$
$[\text{L7Er(hfa)}_3]$	$5.3(3) \cdot 10^{-22} [0.140(7)]$	$3.17(3)$	$15.6(7)$	$29(2)$	$1.0(1) \cdot 10^{-6}$	$1.9(2) \cdot 10^{-1}$	$7.3(9) \cdot 10^{-16} [1.9(2) \cdot 10^5]$
$[\text{L8Er(hfa)}_3]$	$4.1(2) \cdot 10^{-22} [0.107(5)]$	$3.18(3)$	$14.5(6)$	$29(2)$	$3.7(4) \cdot 10^{-7}$	$7.2(9) \cdot 10^{-2}$	$2.5(3) \cdot 10^{-16} [6.4(8) \cdot 10^4]$
$[\text{L9Er(hfa)}_3]$	$7.2(4) \cdot 10^{-22} [0.189(9)]$	$3.36(3)$	$9.1(4)$	$29(2)$	$1.6(2) \cdot 10^{-8}$	$5.1(6) \cdot 10^{-3}$	$1.7(2) \cdot 10^{-17} [4.4(5) \cdot 10^3]$

[a]  $\mathcal{E}^{i \rightarrow j} = 2.6 \times 10^{20} \sigma_{\text{Er}}^{0 \rightarrow 1}$  are given in  $\text{M}^{-1} \cdot \text{cm}^{-1}$  between brackets. [b]  $k_{\text{Er}}^{1 \rightarrow 0} = 1 / \tau_{\text{tot}}^{4\text{I}_{13/2}}$  from Table 1 column 8. [c]  $k_{\text{Er}}^{2 \rightarrow 0} \approx 1 / \tau_{\text{rad}}^{4\text{S}_{3/2}}$  (see main text). [d]  $k_{\text{Er}}^{2 \rightarrow 1} = 1 / \tau_{\text{tot}}^{4\text{S}_{3/2}} - 1 / \tau_{\text{rad}}^{4\text{S}_{3/2}}$  with  $\tau_{\text{tot}}^{4\text{S}_{3/2}} = 20(2) \text{ ns}$  for  $[\text{Er(Et-bzimpy)}_3]^{3+}$  and  $\tau_{\text{tot}}^{4\text{S}_{3/2}} = 3.5(2) \text{ ns}$  for the heteroleptic complexes. [e]  $\lambda_{\text{exc}} = 801 \text{ nm}$  ( $\tilde{\nu}_{\text{exc}} = 12484 \text{ cm}^{-1}$ ) and  $P = 25 \text{ W} \cdot \text{cm}^{-2}$ . [f]  $\eta_{\text{exc}} = \phi_{\text{tot}}^{\text{up}} / \phi_{\text{Er}}^{4\text{S}_{3/2}} = \phi_{\text{tot}}^{\text{up}} (k_{\text{Er}}^{2 \rightarrow 1} + k_{\text{Er}}^{2 \rightarrow 0}) / k_{\text{Er}}^{2 \rightarrow 0}$  (see eq 2). [g] Computed by using  $k_{\text{Er}}^{\text{exc}(1 \rightarrow 2)} = \frac{\lambda_p}{hc} P \sigma_{\text{Er}}^{1 \rightarrow 2} = k_{\text{Er}}^{1 \rightarrow 0} \left( \frac{\eta_{\text{ESA}}}{1 - \eta_{\text{ESA}}} \right)$  (eq 5).

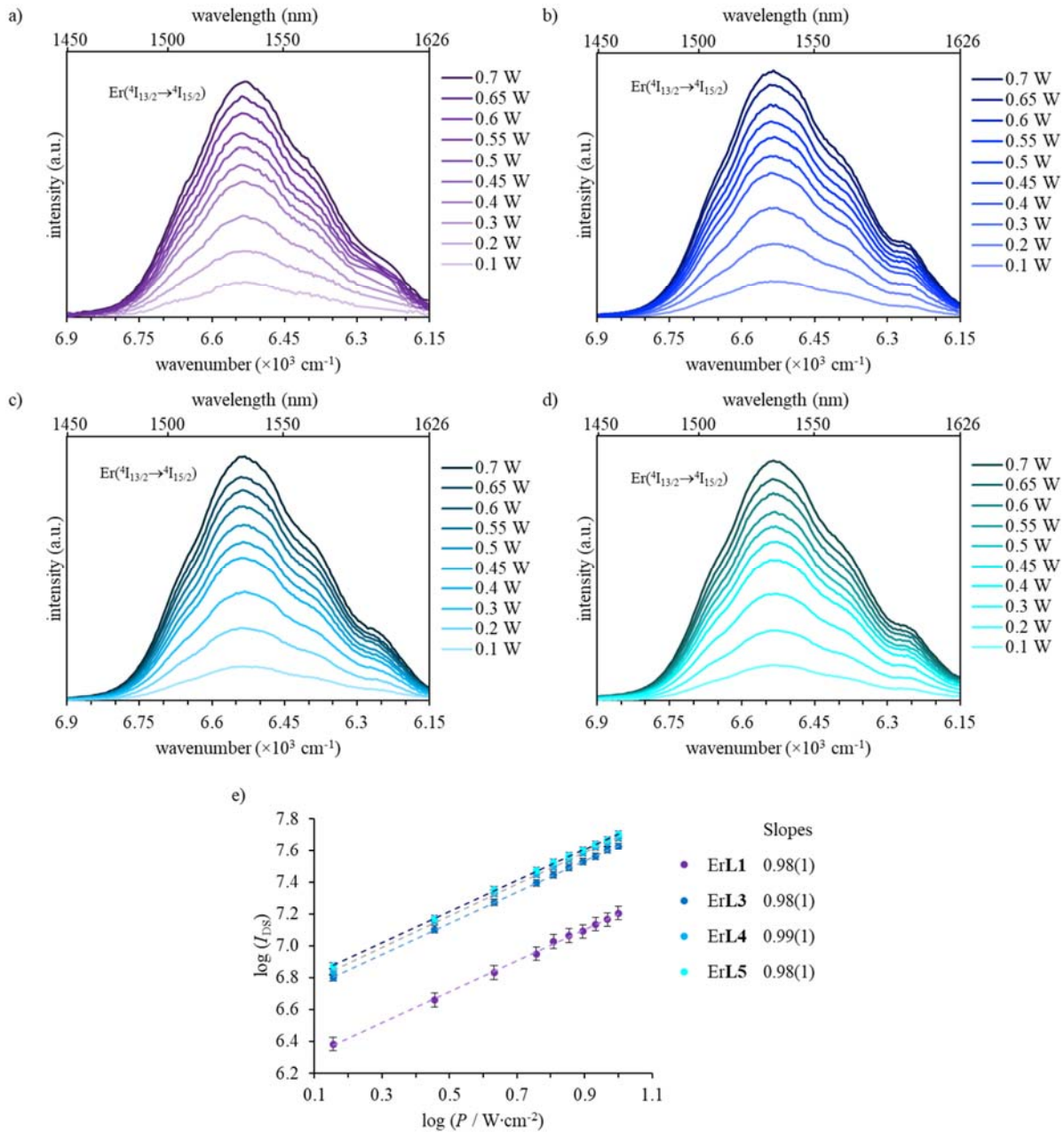


**Figure S14.** Near-infrared downshifted  $\text{Er}(4\text{I}_{13/2} \rightarrow 4\text{I}_{15/2})$  emission observed for  $[\mathbf{Lk}\text{Er}(\text{hfa})_3]$  with a) **L1**, b) **L3**, c) **L4**, and d) **L5** in CH<sub>2</sub>Cl<sub>2</sub> solution (5 mM) at room temperature upon laser excitation of the  $\text{Er}(4\text{I}_{9/2} \leftarrow 4\text{I}_{15/2})$  transition at  $\lambda_{\text{exc}} = 801 \text{ nm}$  ( $\tilde{\nu}_{\text{exc}} = 12284 \text{ cm}^{-1}$ ) and for different incident pump intensities focused on a spot size of  $\approx 0.07 \text{ cm}^2$ . e) Corresponding log–log plot of the downshifted intensities  $I_{\text{DS}}$  as a function of incident pump intensities  $P$  (in  $\text{W} \cdot \text{cm}^{-2}$ ).

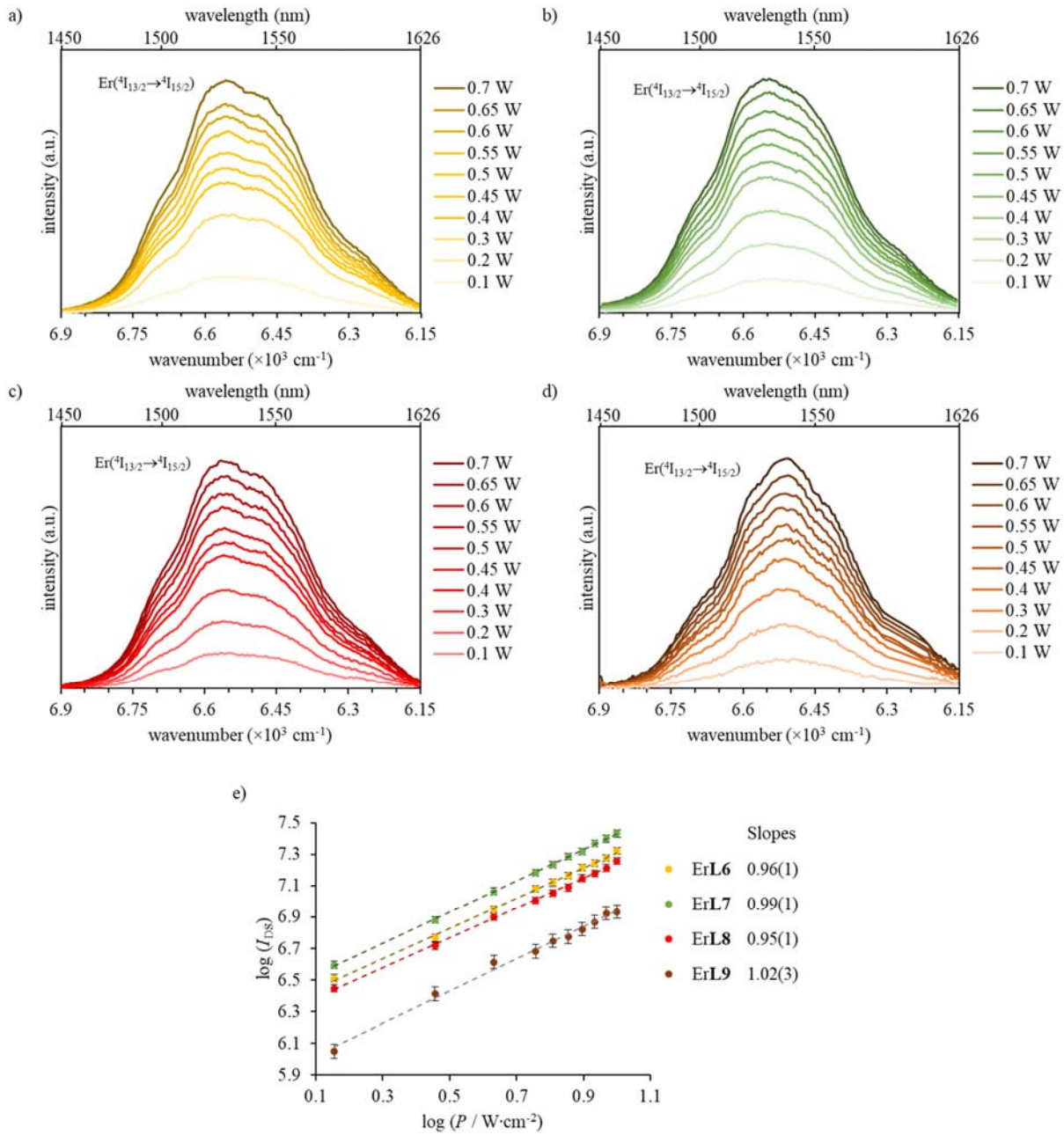


**Figure S15.** Near-infrared downshifted  $\text{Er}({}^4\text{I}_{13/2} \rightarrow {}^4\text{I}_{15/2})$  emission observed for  $[\text{LkEr(hfa)}_3]$  with a) **L6**, b) **L7**, c) **L8**, and d) **L9** in  $\text{CH}_2\text{Cl}_2$  solution (5 mM) at room temperature upon laser excitation of the  $\text{Er}({}^4\text{I}_{9/2} \leftarrow {}^4\text{I}_{15/2})$  transition at  $\lambda_{\text{exc}} = 801 \text{ nm}$  ( $\tilde{\nu}_{\text{exc}} = 12284 \text{ cm}^{-1}$ ) and for different incident pump intensities focused on a spot size of  $\approx 0.07 \text{ cm}^2$ . e) corresponding log–log plot of downshifted intensities  $I_{\text{DS}}$  as a function of incident pump intensities  $P$  (in  $\text{W} \cdot \text{cm}^{-2}$ ).

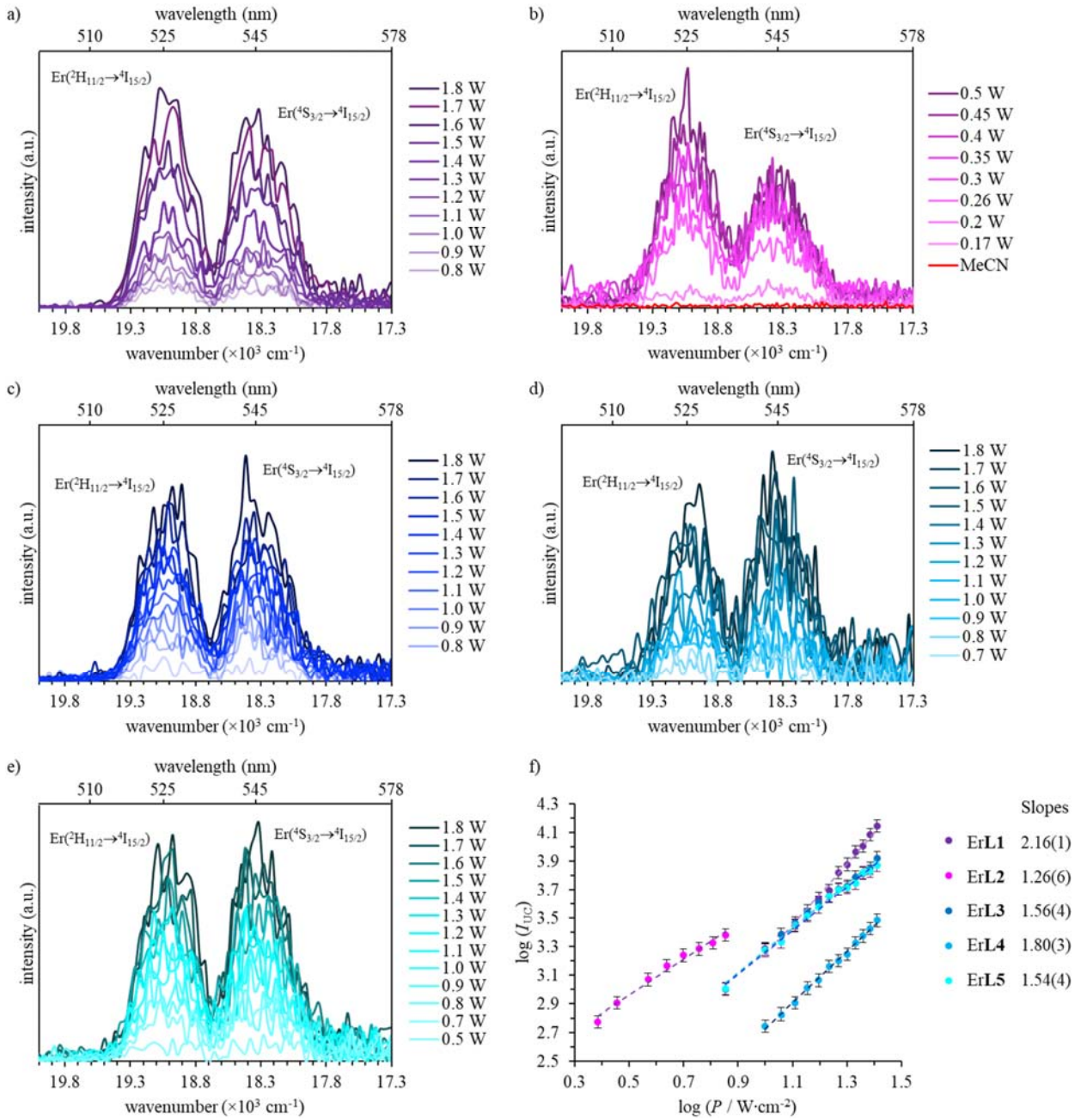


**Figure S16.** Upconverted visible  $\text{Er}(^2\text{H}_{11/2} \rightarrow ^4\text{I}_{15/2})$  and  $\text{Er}(^4\text{S}_{3/2} \rightarrow ^4\text{I}_{15/2})$  emissions observed for  $[\text{LkEr(hfa)}_3]$  with a) L1, c) L3, d) L4 and e) L5 in  $\text{CH}_2\text{Cl}_2$  (5 mM) and b) L2 in  $\text{CH}_3\text{CN}$  (10 mM) solution) at room temperature recorded upon laser excitation of the  $\text{Er}(^4\text{I}_{9/2} \leftarrow ^4\text{I}_{15/2})$  transition at  $\lambda_{\text{exc}} = 801 \text{ nm}$  ( $\tilde{\nu}_{\text{exc}} = 12284 \text{ cm}^{-1}$ ) and using increasing incident pump intensities focused on a spot size of  $\approx 0.07 \text{ cm}^2$  (the blank (red line) was recorded upon irradiation of the DCM or MeCN solution at maximum intensity  $P = 25$  or  $21 \text{ W} \cdot \text{cm}^{-2}$ ) and f) corresponding log–log plot of upconverted intensities  $I_{UC}$  as a function of incident pump intensities  $P$  (in  $\text{W} \cdot \text{cm}^{-2}$ ).

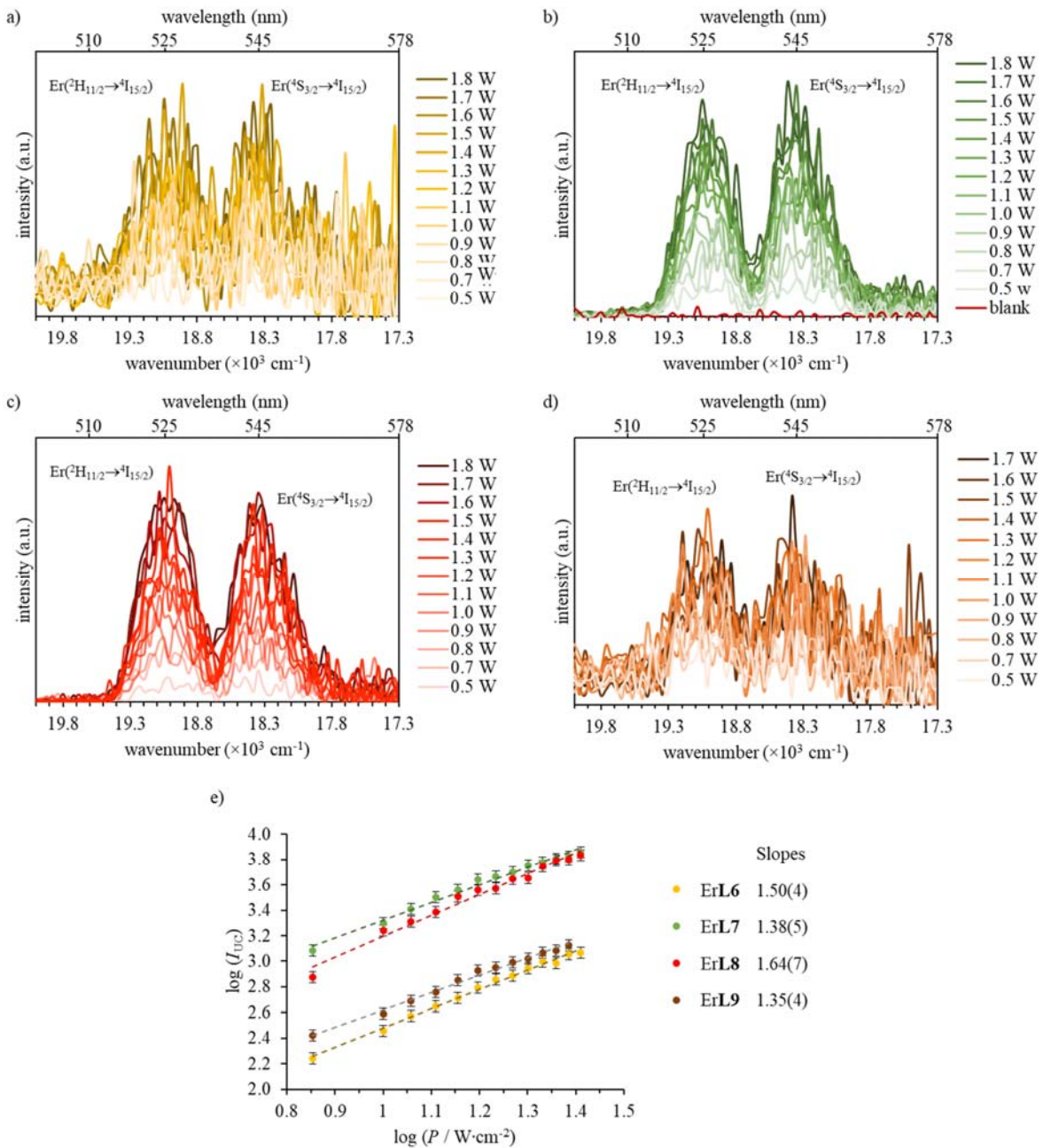


**Figure S17.** Upconverted visible  $\text{Er}(^2\text{H}_{11/2} \rightarrow ^4\text{I}_{15/2})$  and  $\text{Er}(^4\text{S}_{3/2} \rightarrow ^4\text{I}_{15/2})$  emissions observed for  $[\text{LkEr(hfa)}_3]$  with a) L6, b) L7, c) L8, and d) L9 in  $\text{CH}_2\text{Cl}_2$  (5 mM) at room temperature recorded upon laser excitation of the  $\text{Er}(^4\text{I}_{9/2} \leftarrow ^4\text{I}_{15/2})$  transition at  $\lambda_{\text{exc}} = 801 \text{ nm}$  ( $\tilde{\nu}_{\text{exc}} = 12284 \text{ cm}^{-1}$ ) and using increasing incident pump intensities focused on a spot size of  $\approx 0.07 \text{ cm}^2$  (the blank (red line) was recorded upon irradiation of the DCM solution at maximum intensity  $P = 25 \text{ W} \cdot \text{cm}^{-2}$ ) and e) corresponding log-log plot of upconverted intensities  $I_{\text{UC}}$  as a function of incident pump intensities  $P$  (in  $\text{W} \cdot \text{cm}^{-2}$ ).

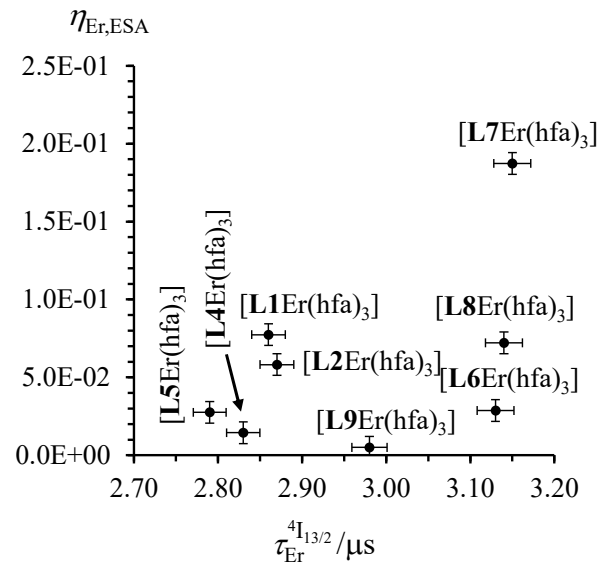


**Figure S18.** Absence of correlation between the upconversion efficiency ( $\eta_{\text{Er,ESA}}$ ) and the total lifetime of the intermediate  $\text{Er}({}^4\text{I}_{3/2})$  excited state (eq 5) for  $[\text{L}k\text{Er}(\text{hfa})_3]$  in dichloromethane solutions.